EGG-CAAP-5189

June 1980

# CALCULATIONS OF A LARGE COLD LEG BREAK WITH STEAM GENERATOR TUBE RUPTURES IN A PWR USING THE TRAC-P1A COMPUTER PROGRAM

J. R. Larson

U.S. Department of Energy
Idaho Operations Office • Idaho National Engineering Laboratory

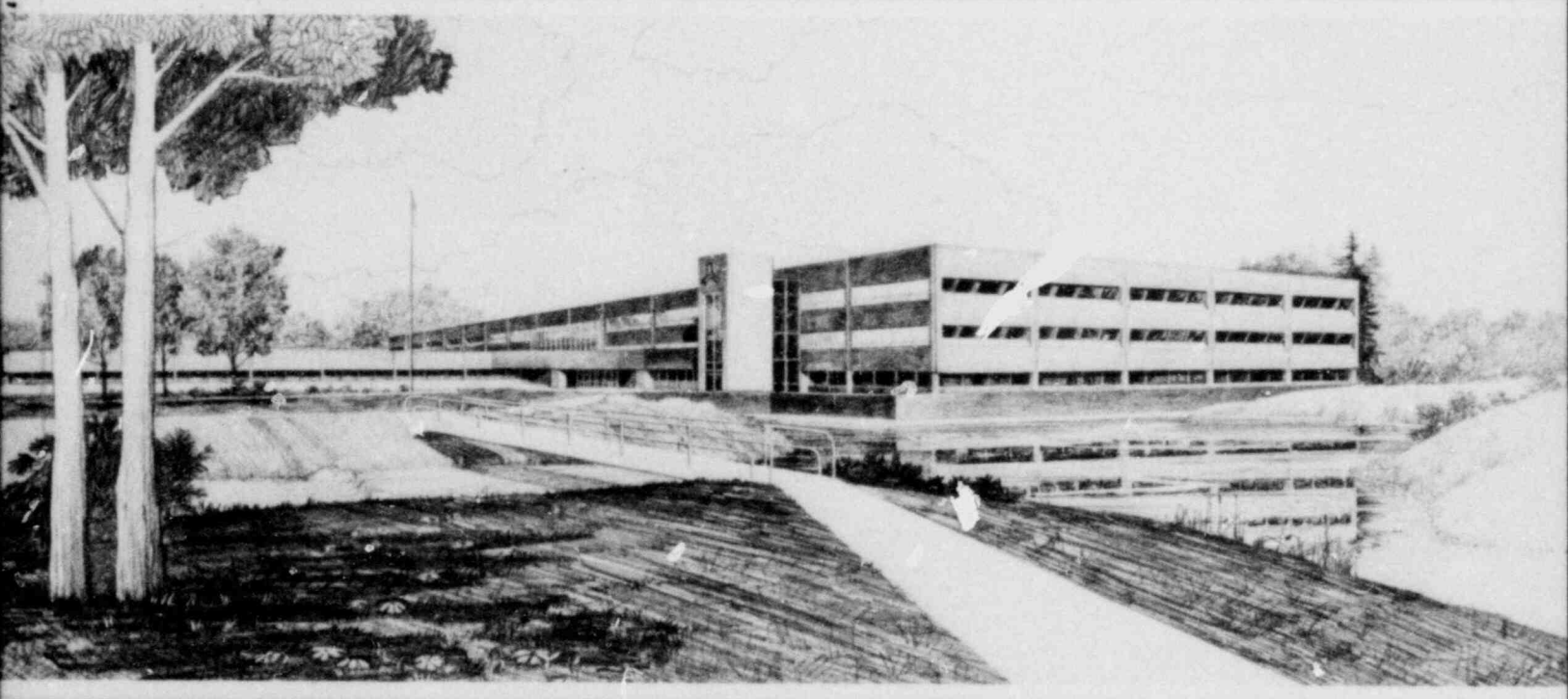



Prepared for the
U.S. Nuclear Regulatory Commission
Under DOE Contract No. DE-AC07-76ID01570
NRC FIN No. A6047

EG&G Idaho

EG&G Idaho, Inc.

FORM EG&G-398
(Rev. 11-79)



**INTERIM REPORT**

Accession No. _____

Report No. EGG-CAAP-5139

**Contract Program or Project Title:** Code Assessment and Applications Program

**Subject of this Document:** Calculations of a Large Cold Leg Break with Steam Generator Tube Ruptures in a PWR Using the TRAC-P1A Computer Program

**Type of Document:** Preliminary Assessment Report

**Author(s):** J. R. Larson

**Date of Document:** June 1980

**Responsible NRC Individual and NRC Office or Division:** F. Odar, NRC-RSR



EG&G Idaho, Inc.
Idaho Falls, Idaho 83415

Prepared for the
U.S. Nuclear Regulatory Commission
Washington, D.C.
Under DOE Contract No. DE-AC07-76ID01570
NRC FIN No. A6047

**INTERIM REPORT**

## ABSTRACT

Calculations were made with the TRAC-P1A system thermal-hydraulic computer program for a postulated double ended cold leg break LOCA including rupture of a number of steam generator tubes. Two calculations were made with the rupture flow rate sized to approximate the condition where cladding temperature showed the largest increase in Semiscale Mod-1 tests and to approximate the largest rupture flow rate tested in the Semiscale Mod-1 tests. The calculations were described and qualitatively compared to the existing data.

ACKNOWLEDGEMENT

The author wishes to acknowledge D. L. Terry and C. Polk for their help in preparing the figures, J. M. Mosher who prepared the text, and to A. C. Peterson, Jr., for a critical review of the discussion presented.

CONTENTS

FIGURES

TABLES

## SUMMARY

Calculations were made with the TRAC-P1A computer program for a double-ended cold leg break including rupture of a number of steam generator tubes permitting fluid flow from the secondary to the primary side during a postulated LOCA transient. The specific objectives of this task were to determine if the detailed calculations for the system hydraulic and core thermal response could be accomplished, find if three dimensional effects occurred in the upper plenum because of the ruptured tubes and compare the calculations to the Semiscale Mod-1 data.

Two calculations were performed, one for a small number of ruptured tubes and one for a large number of ruptured tubes, each sized to obtain an appropriate scaled mass flow rate from the secondary side to the primary side. The mass flow rate for the small number of ruptured tubes was selected to be equivalent to the mass flow rate found to cause the largest increase in cladding temperature during the Semiscale Mod-1 tests. The mass flow rate for the large number of ruptured tubes was selected to be equivalent to the largest rate tested in the Mod-1 system. The mass flow rate values were scaled by using the ratio of the core flow areas of a PWR and the Semiscale Mod-1 system.

Information about the Zion I pressurized water reactor provided input to the analytical model. Several sources were used to obtain the required information. The model explicitly represented a postulated broken loop and three intact loops. One intact loop contained the flow path simulating the ruptured steam generator tubes and another intact loop contained the pressurizer. The vessel was divided into 12 axial levels (3 levels for the lower plenum, 5 levels for the core, 3 levels for the upper plenum and 1 level for the upper head), three rings (2 rings for the core and 1 ring for the downcomer) and 8 azimuthal segments.

The calculated results for the small number of ruptured tubes were compared to the results obtained in companion studies for a double ended

cold leg break without ruptured tubes during the first 30 s of the transient. The results for the two calculations were found to be very similar until the time the loop containing the rupture became blocked to normal flow, that is flow in the hot leg piping reversed direction at the location where the rupture flow entered the primary piping and traveled into the upper plenum. Roughly half of the flow from the rupture entered the upper plenum, maintaining the upper plenum at a higher pressure than for the calculation with no rupture. The liquid and vapor phases separated upon entering the upper plenum with the liquid flowing preferentially to the vessel inner ring cell opposite the hot leg piping-vessel junction, down through the core and into the lower plenum. Sufficient vapor flow continued up the downcomer and reduced the accumulator injection liquid which reached the lower plenum for the small rupture calculation compared to the calculation without ruptured tubes.

The calculation for the small number of ruptured tubes indicated that accumulator liquid continued to bypass the lower plenum and was forced out the broken cold leg. Thus, at the end of accumulator injection the lower plenum was only 60% liquid full. For the calculation without ruptured tubes the lower plenum was filled and liquid forced into the core by the accumulator gas discharge which began the bottom flooding process.

After accumulator gas discharge, the calculation for the small number of ruptured tubes indicated a gradual refill of the lower plenum with liquid furnished by the ECC systems. The preferential down flow in the inner ring cell provided significant cooling to the fuel rods but not enough to quench the rods. With eventual refill of the lower plenum the bottom flooding process began and the increase in cladding temperature was arrested.

For the calculation with the large number of ruptured tubes the rupture mass flow prevented the liquid from the accumulators from reaching the lower plenum. A falling film quench front was initiated in several cells, primarily at the location of the large preferential downward flow.

As the flow rate from the ruptured tubes diminished because of mass depletion in the secondary side of the steam generator, the vapor velocity up the downcomer decreased and permitted countercurrent flow of ECC liquid into the lower plenum. Also, as the flow rate from the ruptured tubes decreased the falling film quench position on the rods other than those in the preferential flow path retreated. The calculation for the large number of ruptured tubes was terminated prior to commencement of bottom flooding. However, it appeared that refill would have been completed prior to achieving cladding temperatures in excess of those calculated for the small number of ruptured tubes.

The calculated behavior for the system hydraulic and core thermal response was compared to Semiscale Mod-1 data. The system hydraulic response was approximately the same for the calculations and the data. Some differences in event timing occurred because the accumulator model resulted in too large a mass flow rate exiting the accumulator and gas discharge thus occurred earlier in the calculation than for the data.

The core thermal response showed major differences between the calculations and the data. Data for the small number of ruptured tubes indicated quenching of a few rods near a preferential flow path located on the vessel wall prior to bottom flooding; this was not noted in the calculation. Also data for the large number of ruptured tubes indicated quenching completed prior to bottom flooding, but for the calculation a significant quench had occurred only on the rods exposed to the preferential flow.

In conclusion, the TRAC-P1A program proved capable of making calculations to predict the behavior for a postulated cold leg break with the addition of rupture of a number of steam generator tubes. The calculated system hydraulic behavior agreed reasonably well with data whereas some differences existed in the core thermal response between the calculation and data. Significant three dimensional flow effects were calculated for the upper plenum.

# 1. INTRODUCTION

Calculations have been performed for a typical PWR with the TRAC-P1A[1] computer program over a range of postulated LOCA break conditions to determine the general behavior of the code, to obtain baseline information for use in further studies, and to determine areas where additional code development or modeling studies might be desirable. The calculations encompass hot and cold leg locations, full to small sizes, and with the inclusion of steam generator tube rupture as an additional parameter. The calculations cover the blowdown, refill and reflooding phases of the accident.

This report describes the calculated results for a double-ended cold leg break with rupture of a number of steam generator tubes permitting fluid flow from the steam generator secondary side to the primary side during the LOCA transient. The specific objectives of this task were to determine if the detailed thermal-hydraulic calculation could be accomplished, if three dimensional effects occurred in the upper plenum because of the rupture flow and to compare the calculations with available data. Other reports describe the results for a large, an intermediate and a small cold leg break[2] and for a large hot leg break and a large hot leg break with the inclusion of ruptured steam generator tubes.[3]

The effect of ruptured steam generator tubes was previously investigated analytically with the FLOOD4 code and experimentally in the Semiscale Mod-1 test apparatus.[4] (The Semiscale Mod-1 system consisted of an intact loop representing three loops and a broken loop.) Analytically and experimentally the secondary to primary flow was simulated by injecting liquid into the intact loop hot leg between the steam generator inlet plenum and the pressurizer. The injection was accomplished by using a constant pressure water source with the water at a temperature typical of a steady state PWR steam generator fluid temperature. The injection was initiated at the beginning of the refill or reflood phase of the accident.

The Semiscale analyses and experiments both indicated that a relatively narrow range of simulated tube rupture mass flow rates (mass flow rate scaled to approximate the flow rate of 16 ruptured tubes in a PWR steam generator) would result in increased peak cladding temperatures by delaying ECC penetration of the downcomer and lower plenum thus delaying core reflood. Larger mass flow rates (rates scaled to be equivalent to 60 ruptured tubes) delayed refill but permitted quenching from the top of the core with the net result that increased cladding temperatures were not obtained.

Descriptions of the code, model nodalization, code options and initial conditions are found in Section 2. Section 3 includes the results for calculations made for the worst case mass flow rate found in the Semiscale tests (that is, resulting in the maximum cladding temperature and termed the small rupture calculation) and for the upper bound of mass flow rates tested (termed the large rupture calculation). The results of these calculations are compared to those for a large cold leg break[2] and to the Semiscale Mod-1 results to show where differences and similarities in behavior occur. The conclusions and recommendations of the report are found in Section 4 and the references in Section 5. Appendix A presents a detailed discussion of the model nodalization. Appendix B presents detailed component initial and boundary conditions. An input listing is found in Appendix C.

## 2. MODEL DESCRIPTION

The calculational model was developed using the Zion I pressurized water reactor as a basis for providing input to the TRAC computer program. The input data came from three sources, the BE/EM study,[5] a PWR model developed by LASL[1] and the Safety Analysis Report for the Zion I reactor.[6] The BE/EM study was the primary source unless better or more complete information was available elsewhere. The following sections describe the code version used, model nodalization, code options, and the initial and boundary conditions for the calculation. Details concerning the nodalization and boundary conditions of the components are described in Appendix A and B respectively. A detailed listing of the code input is provided in Appendix C.

### 2.1 Code Description

The code version used was TRAC-P1A[2] with the updates described in TRAC Newsletter No. 1.[7] The configuration control number for the code is H003885B. The configuration control number for the steady state model and changes for the transient calculation is H01380IB.

### 2.2 Nodalization

The 200% cold leg break model consisted of four separate loops (one broken and three intact) and a vessel. The four loops were explicitly represented to obtain the specific effect of the pressurizer and ruptured steam generator tubes. The steady state model consisted of 55 components and 548 cells. The transient model included the addition of the breaks and a valve component to simulate the steam tube rupture. The transient model differed slightly from the model of Reference 1 in that two cells were eliminated from the secondary side of the tee components connecting the accumulators and pressurizer to the loops because the model exceeded the allowable computer storage capacity. The number of cells was 550 for the transient model with 57 components. For comparison the USPWR1 model

developed by LASL consisted of 42 components and 634 cells. Additional cells were required in the USPWR1 model vessel because it consisted of 5 rings.

Figure 1 shows the nodalization of the loops and vessel level 10 where the loops connect to the vessel for the transient model. Steady state calculations were made by elimination of the BREAK components 47 and 48 and joining component TEE 49 and component PIPE 6, removal of VALVE 61 and adding FILL 18. Loop 1 contained the breaks and also contained all of the regular loop components.

Primary flow left the vessel through PIPE 1, connecting to the primary side of the "U" tube STEAM GENERATOR 2. The secondary side of the steam generator was supplied with feedwater through FILL 7. The vapor leaving the steam generator exited through VALVE 62 and BREAK 48. VALVE 62 was closed shortly after the commencement of the transient to prevent backflow into the secondary side once the pressure dropped below the break pressure.

The primary flow exited the steam generator through PIPE 3, and PUMP 4. TEE 5 provided the injection location for ACCUMULATOR 10. VALVE 9 was the check valve isolating the accumulator from the primary loop piping. The low and high pressure injection systems entered TEE 49 through FILL 11.

Loop 2 contained the steam generator tube rupture flow path simulated by VALVE 61 which replaced the FILL 18 used during steady state. VALVE 61 connected the steam generator secondary side to the primary loop piping upstream of the steam generator inlet. Loop 4 contained the PRESSURIZER 45.

The axial and radial noding of the vessel is shown in Figure 2. The nodalization consisted of 12 axial levels with each level subdivided into 3 radial and 8 azimuthal zones for a total of 288 mesh cells. Three radial zones were the minimum required to represent a core radial power distribution and the downcomer. The bottom of the downcomer was at the top

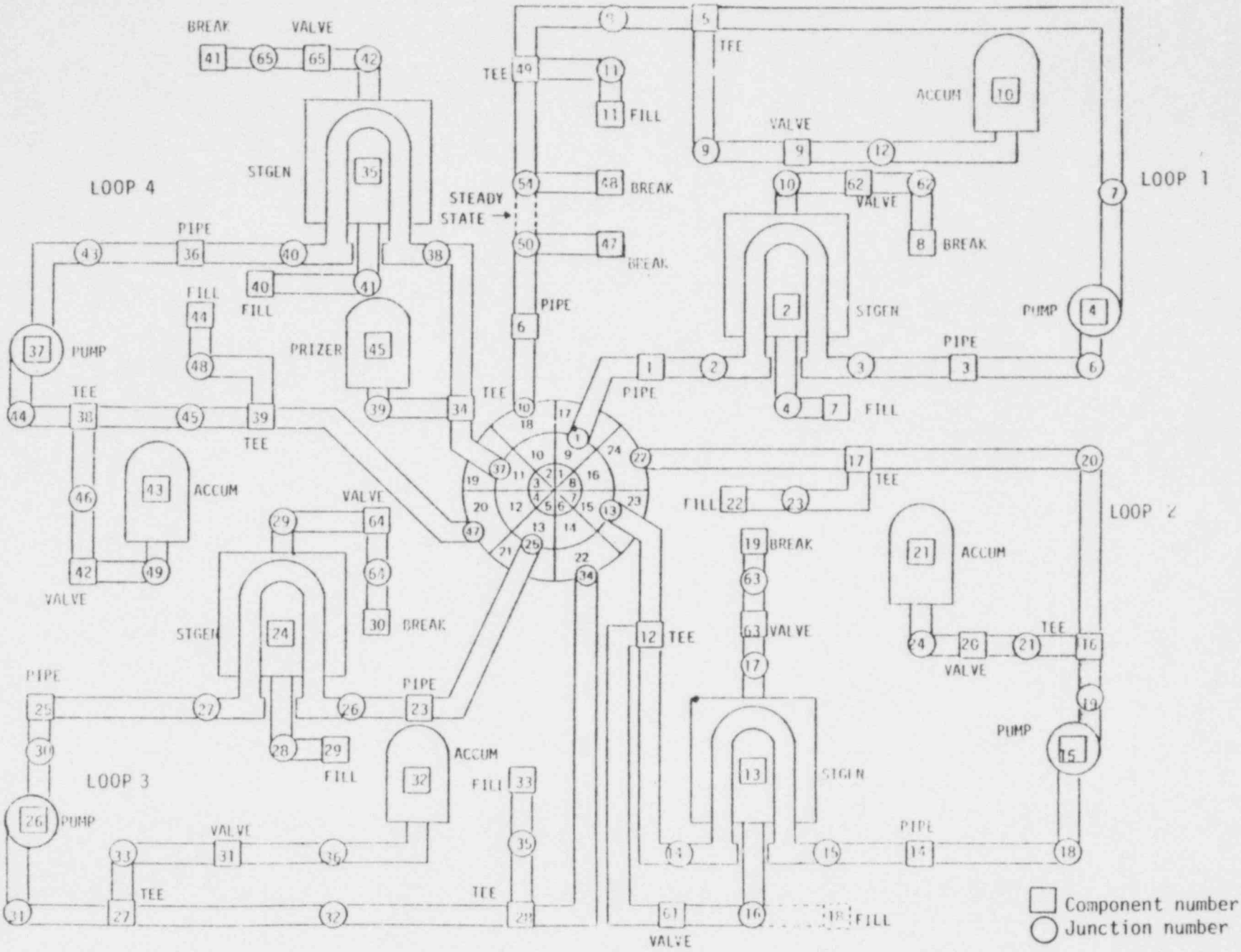


Figure 1. Nodalization of loops and vessel level 10 for transient calculations.

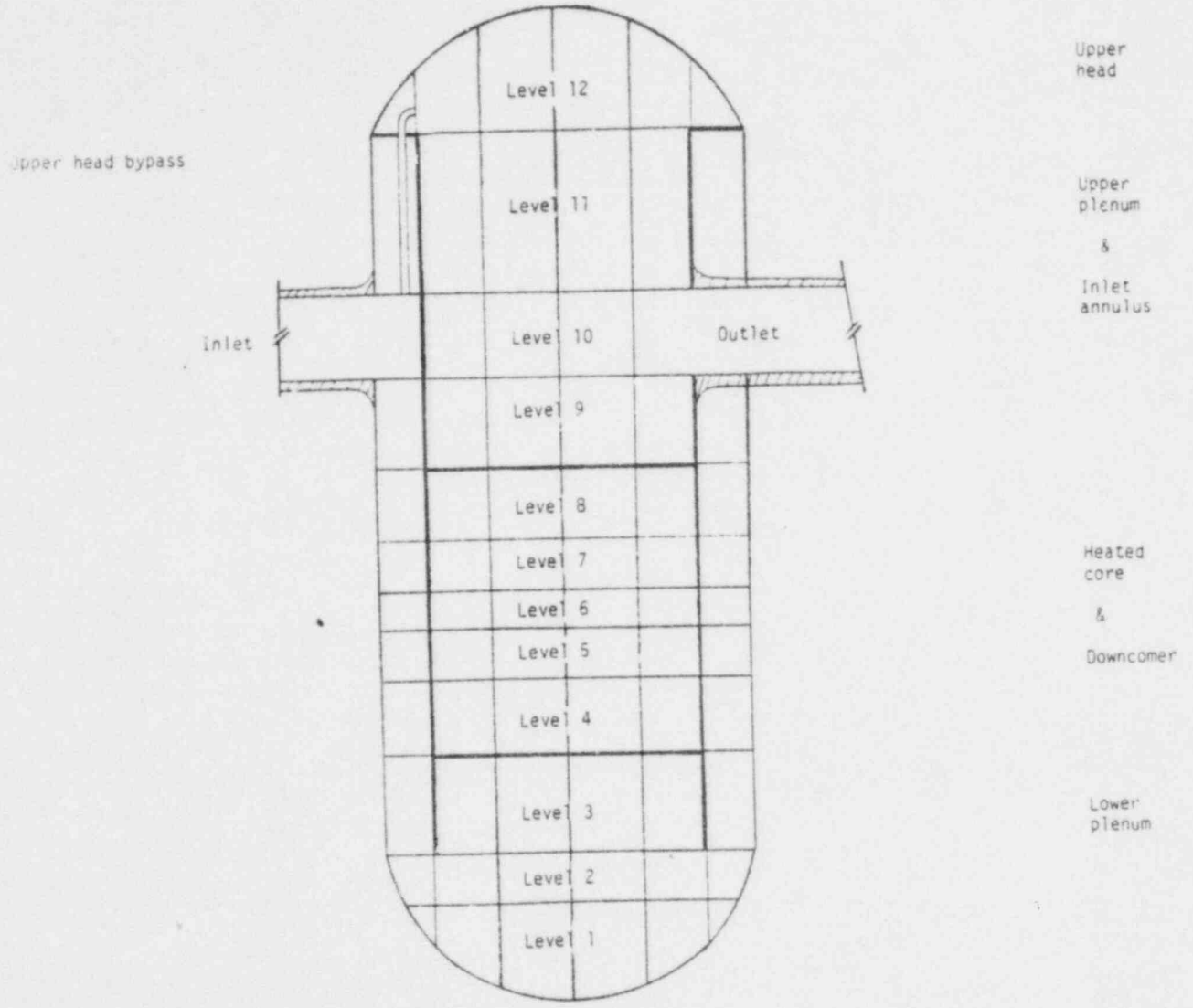


Figure 2. Axial and radial nodalization of the vessel.

of vessel level 2. The lower plenum consisted of three levels with the top being the lower end of the active portion of the fuel rod. The core consisted of 5 levels encompassing only the active fuel. The upper plenum consisted of three levels, the middle level spanning the hot leg pipes shown as one outlet. One level represented the upper head.

Descriptions of the vessel, pressurizer, accumulators, breaks, ECC injection, steam generator and VALVE 61 may be found in Appendix A.

## 2.3 Code Options

Few code options exist in TRAC-P1A. A major choice concerns the friction factor correlation to be used in components other than the vessel. Based on the TRAC Developmental Assessment Report,[8] the annular flow correlation (NFF=4) was selected for all components except VALVE 61. The homogeneous flow correlation (NFF=1) was used in VALVE 61 because the area of the nozzle to simulate the steam generator tube rupture was evaluated using that correlation.

The option permitting the code to calculate the fuel rod gap conductance was also selected (NFCI=1). This resulted in a lower than reasonable gap conductance and an excessively high peak centerline temperature. The effect of this parameter on cladding surface temperature is discussed in a companion report.[2] The net result was to lower the clad surface temperature about 200 K at 40 s.

The option for determining core power versus time (IRPOP=7) was selected. The power-time table was taken from the BE/EM study.

The partially implicit numerical hydrodynamics option (IHYDRO=0) was used throughout the loop piping except for the piping adjacent to the breaks where the fully implicit option (IHYDRO=1) was used. The fully implicit option was also used on the secondary side of the tees connecting the pressurizer and accumulator to the loop.

## 2.4 Initial and Boundary Conditions

The system operating conditions are shown in Table 1. Appendix B describes the initial and boundary conditions applied to the model components in more detail.

TABLE 1. SYSTEM OPERATING CONDITIONS

| | |
|---|---|
| Core power (MWt) | 3228 |
| Loop Mass Flow Rate (kg/s) | |
| Loop 1 | 4615 |
| Loop 2 | 4614 |
| Loop 3 | 4613 |
| Loop 4 | 4601 |
| Hot Leg Entrance Temperature (K) | |
| Loop 1 | 583.2 |
| Loop 2 | 583.0 |
| Loop 3 | 583.2 |
| Loop 4 | 583.2 |
| Cold Leg Exit Temperature (K) | |
| Loop 1 | 550.5 |
| Loop 2 | 550.5 |
| Loop 3 | 550.6 |
| Loop 4 | 550.5 |
| Pump Head (MPa) | |
| Loop 1 | 0.606 |
| Loop 2 | 0.644 |
| Loop 3 | 0.644 |
| Loop 4 | 0.618 |
| Upper Head Temperature | 569.4 |
| Core $\Delta T$ (K) | 33.2 |
| Core $\Delta P$ (MPa) | 0.085 |
| Average Rod Peak Power Rating (kw/m) | 31.73 |

# 3. RESULTS

This section describes the calculated results for a postulated LOCA in a PWR including the effect of ruptured steam generator tubes in one of the loops. The results are presented for a small rupture (mass flow rate from the secondary to primary side scaled to approximate the mass flow rate from 16 ruptured tubes) and a large rupture (mass flow rate scaled to approximate the flow from 60 tubes). Selected results for the small rupture are compared to the results for the large cold leg break without ruptured steam generator tubes. The large rupture results are also compared to the small rupture results.

It is suggested that Reference 2 be reviewed to obtain a perspective of the behavior calculated by TRAC-P1A for a large cold leg break without ruptured steam generator tubes. This report does not describe the complete behavior of the reactor system but is restricted primarily to differences in behavior related to steam generator tube rupture and their cause.

The timing of the major events for the calculations to be compared are shown in Table 2.

## 3.1 Small Rupture

During blowdown differences between the behavior of a PWR large cold leg break with and without ruptured steam generator tubes were slight. The major difference occurred during the refill period which changed the results of the remainder of the transient. The calculated results are first shown for the 0-30 s time period and are compared to the case without steam generator tube ruptures. The long term results are then shown out to 150 s.

### 3.1.1 Small Rupture Short Term Results (0-30 s)

The mass flow rate through the flow path connecting the secondary side of the steam generator to the primary loop is shown in Figure 3. The

TABLE 2. EVENT SEQUENCE FOR LARGE COLD LEG BREAK WITH AND WITHOUT STEAM GENERATOR TUBE RUPTURE AS CALCULATED BY TRAC-P1A

| Event | Time (s) No Rupture | Small Rupture | Large Rupture |
|---|---|---|---|
| Break | 0.0 | 0.0 | 0.,0 |
| Reactor Scram | 0.53 | 0.53 | 0.53 |
| Loop 1 Accumulator Trip | 2.81 | 2.50 | 2.47 |
| ECCS Trip | 3.05 | 3.02 | 3.02 |
| Loop 2 Accumulator Trip | 13.0 | 11.71 | 11.90 |
| Loop 3 Accumulator Trip | 13.0 | 11.77 | 11.96 |
| Loop 4 Accumulator Trip | 13.0 | 11.78 | 11.97 |
| Pressurizer Empty | 16.3[a] | 18.9 | 19.4 |
| Loop 1 Accumulator Empty | 20.0 | 19.8 | 19.6 |
| Loop 2 Accumulator Empty | 26.3 | 26.3 | 27.4 |
| Loop 3 Accumulator Empty | 26.3 | 26.3 | 27.2 |
| Loop 4 Accumulator Empty | 26.3 | 26.3 | 27.4 |
| Start of Refill | 24.3 | 24.0 | 96.0 |
| Lower Plenum Refilled | 28.0 | 92.7 | 200.0[b] |

a. Considered empty when equivalent water level reached 0.1 m.

b. Estimated time.

rupture flow path (VALVE 61 of Figure 1) was open from the beginning of the transient. Delay in opening of the valve until 20 s probably would not have influenced the results as will be shown.

As shown in Figure 3 the flow direction through the small rupture flow path was initially into the secondary side of the steam generator since the primary loop was at a considerably higher pressure. At about 7-1/2 s the pressure in the loop piping equaled the secondary side pressure and then declined at a faster rate. Consequently the flow changed direction and emptied from the secondary side into the primary loop reaching a near constant value near the scaled value of 150 kg/s. The initial fluid mass in the secondary side was sufficient to maintain this flow rate for about 340 s.

The pressure behavior of the bottom cell of the secondary side is shown in Figure 4. The pressure initially decreased slightly while the flow through the primary side oscillated, reducing the heat transfer to the secondary side. At about 1-1/2 s flow out the secondary side exit stopped when the exit, VALVE 62, was closed. At this time the pressure increased primarily through additional heat transfer from the primary side fluid as the primary flow through the loop stabilized in the normal direction. The contribution of the pressure change due to the mass inflow can be seen by comparison to the results for the calculation without ruptured steam generator tubes.

The mass flow rate at the hot-leg vessel junction for loop 2 is shown in Figure 5. The figure compares the flow rate with and without ruptured steam generator tubes. The flow rates were of similar magnitude and direction up to about 20 s when the flow direction differed with part of the flow from the ruptured steam generator tubes entering the vessel and blocking flow through the loop from the upper plenum to the downcomer. Over the time interval 8 to 15 s, the reverse flow into the upper plenum for both calculations was caused by a reversal in heat transfer direction from the steam generator secondary side to the primary side and additional

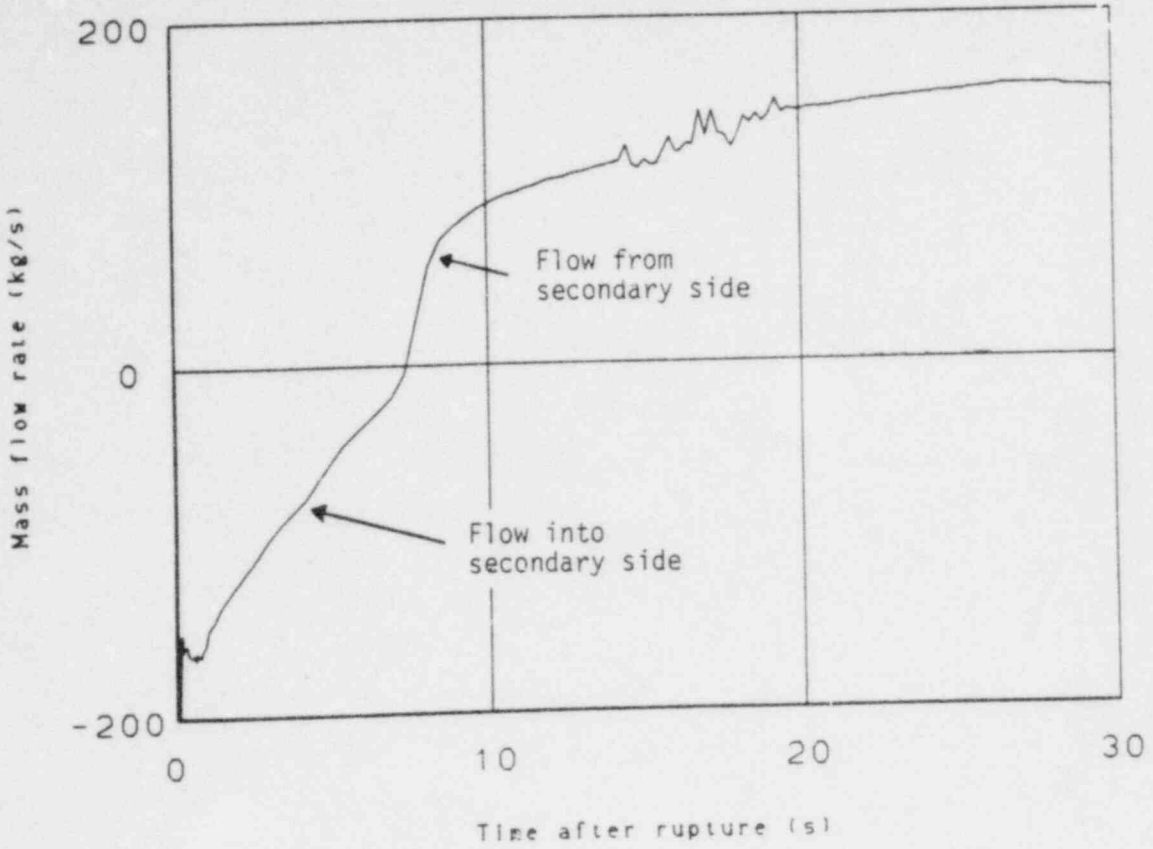


Figure 3. Mass flow rate through the small rupture flow path connecting the steam generator secondary side to the primary loop (0-30 s).

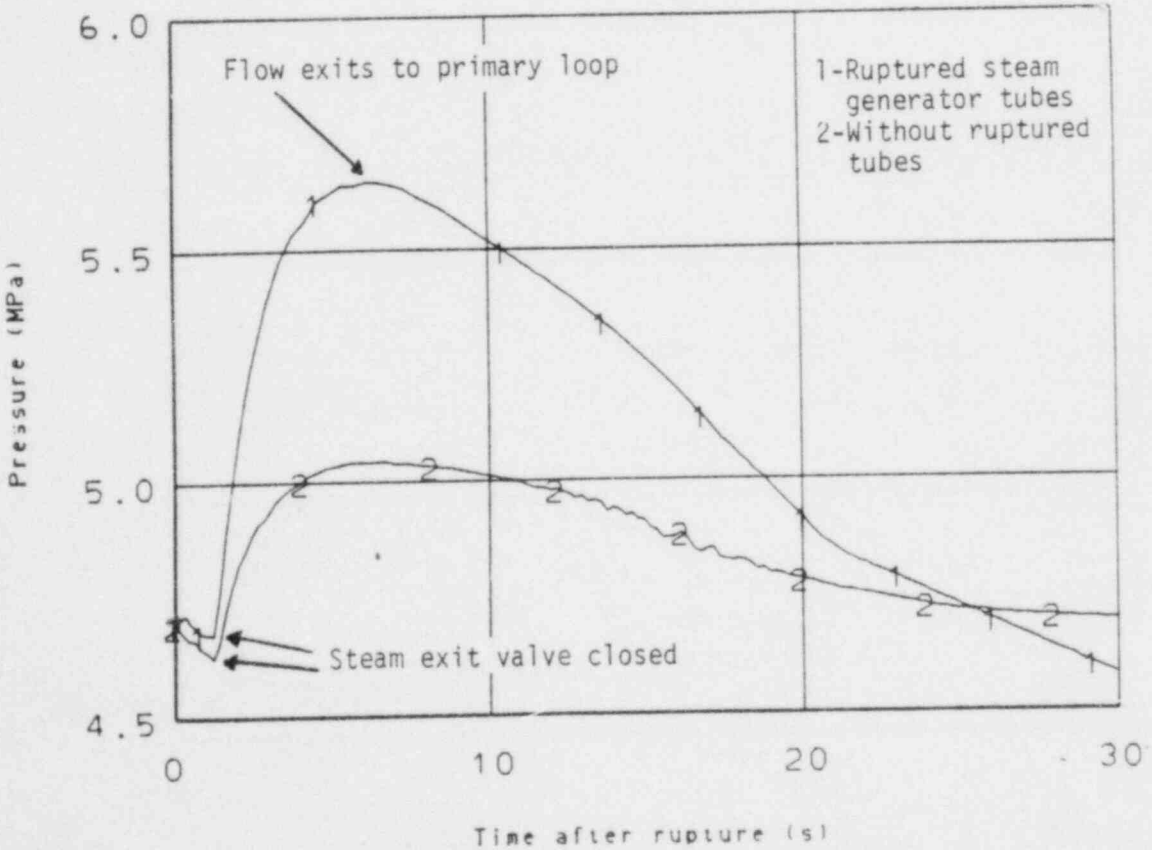


Figure 4. pressure in steam generator component number 13, secondary side cell 1 with and without the small rupture rupture (0-30 s).

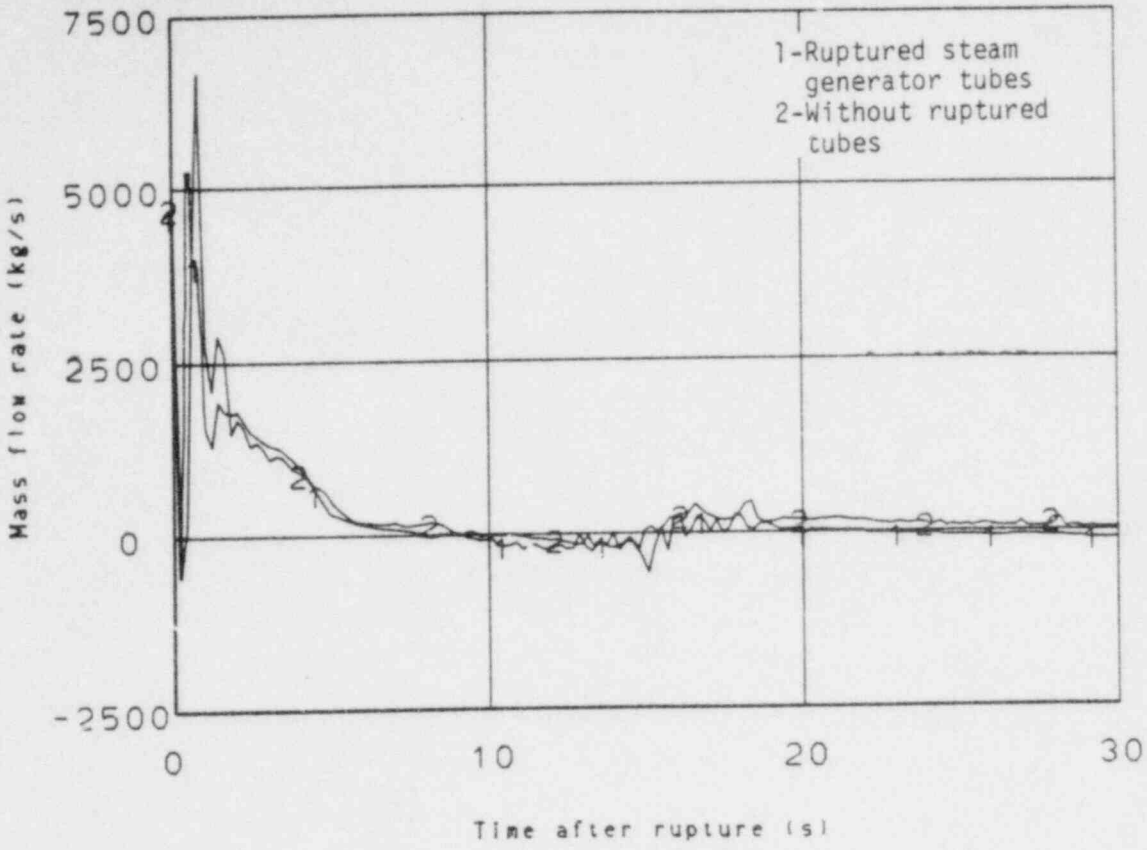


Figure 5a. Mass flow rate at the loop 2 hot leg piping - vessel upper plenum junction with and without the small rupture (0-30 s).

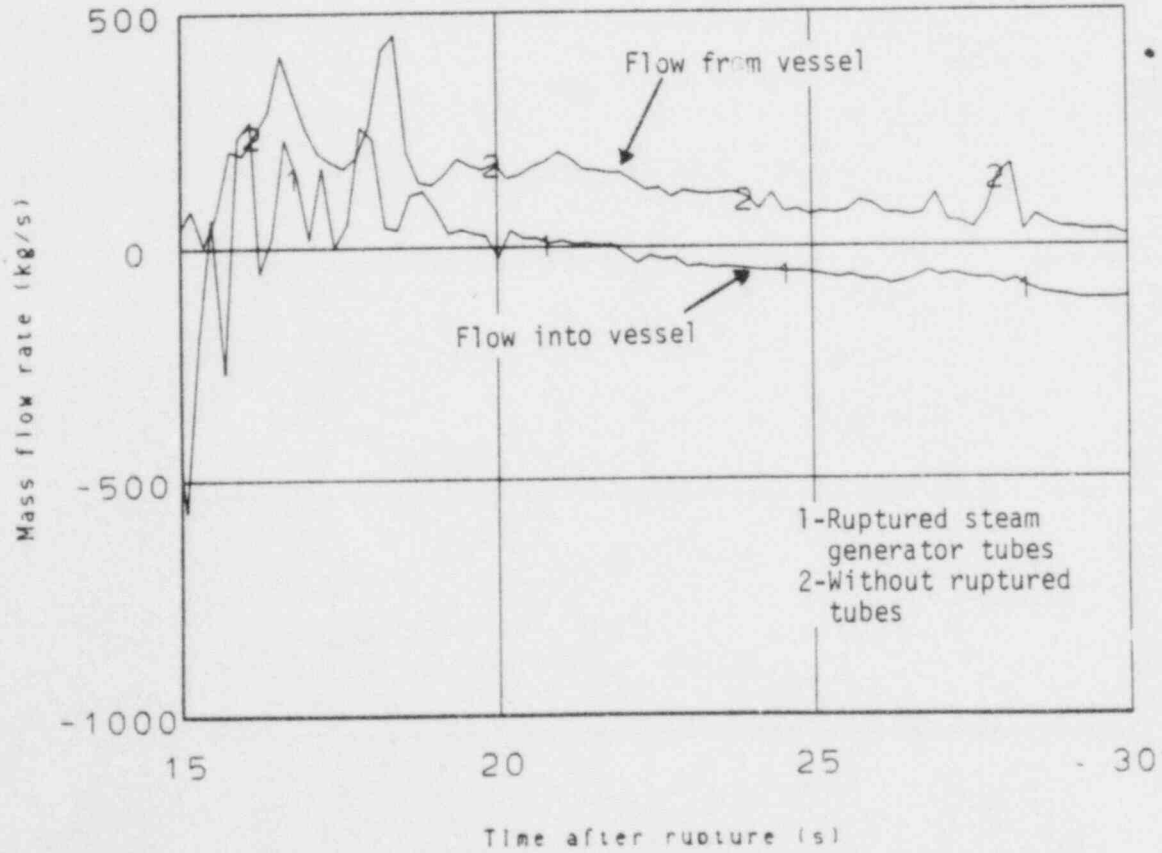


Figure 5b. Mass flow rate at the loop 2 hot leg piping - vessel upper plenum junction with and without the small rupture (15-30 s).

steam generation from depressurization causing flow stagnation in the steam generator tubing. For the calculation with no ruptured steam generator tubes the flow in the loop continued in the normal direction.

During the time period 25 to 28 s about 40 to 50% of the rupture flow traveled through the hot leg piping to the vessel. The remainder traveled around the loop to the downcomer.

The mass flow rate at the loop 2-downcomer junction is shown in Figure 6. For the calculations with and without ruptured steam generator tubes the flows were similar in magnitude and direction indicating that the steam generator rupture flow had little effect on the fluid in the cold leg piping. The mass flow rate for both calculations increased with accumulator injection, peaked when normal flow resumed in loop 4 as the pressurizer emptied[a] and peaked again because of the high volumetric flow of gas out of the accumulator before the code automatically terminated the flow.

The blockage in loop 2 effectively maintained a higher pressure in the upper plenum and downcomer for the calculation with ruptured steam generator tubes when compared to the calculation without rupture tubes. This effect is shown in Figures 7 and 8 from 15 s until core reflooding began at 27.5 s for the calculation without ruptured steam generator tubes.

---

a. Flow from the pressurizer acted to block the normal flow through loop 4 from the upper plenum to the downcomer in a similar manner as the flow from the ruptured steam generator blocked loop 2.

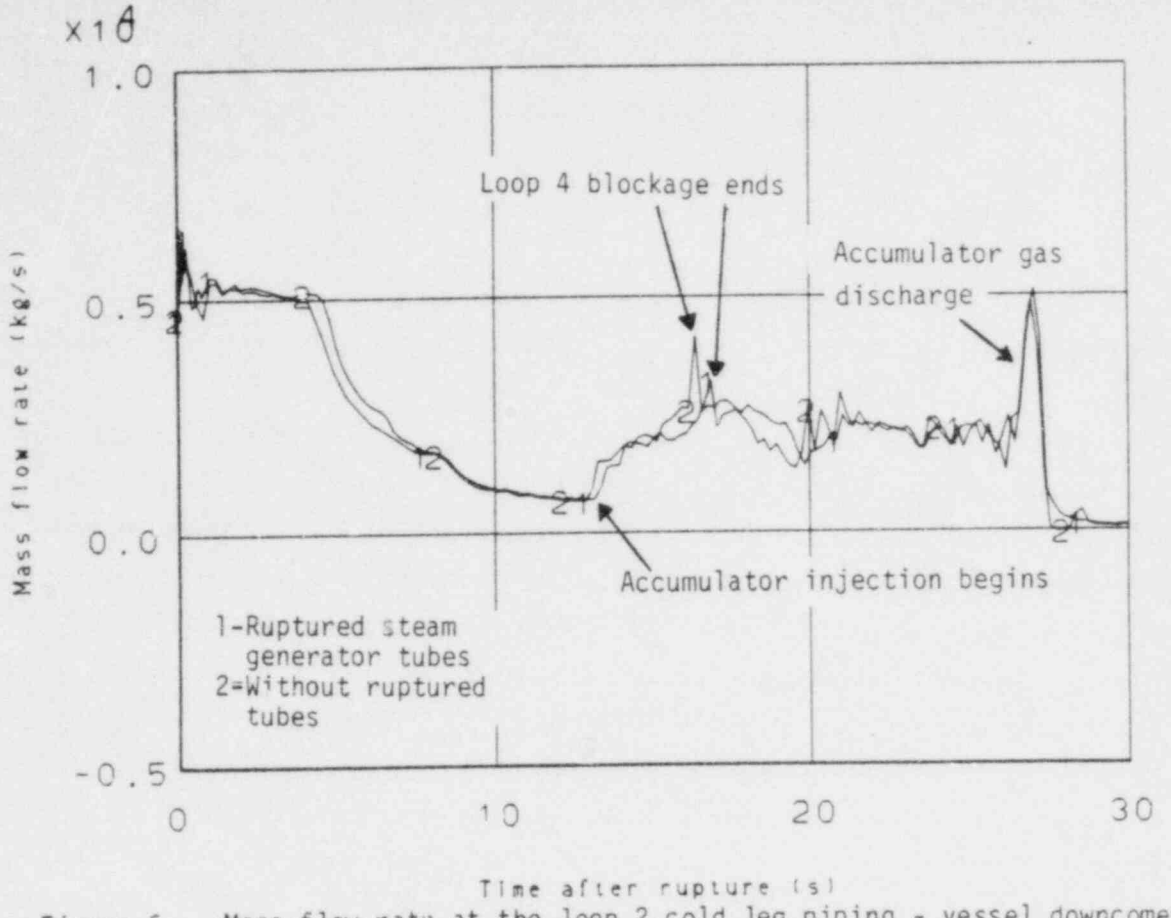


Figure 6. Mass flow rate at the loop 2 cold leg piping - vessel downcomer junction with and without the small rupture (0-30 s).

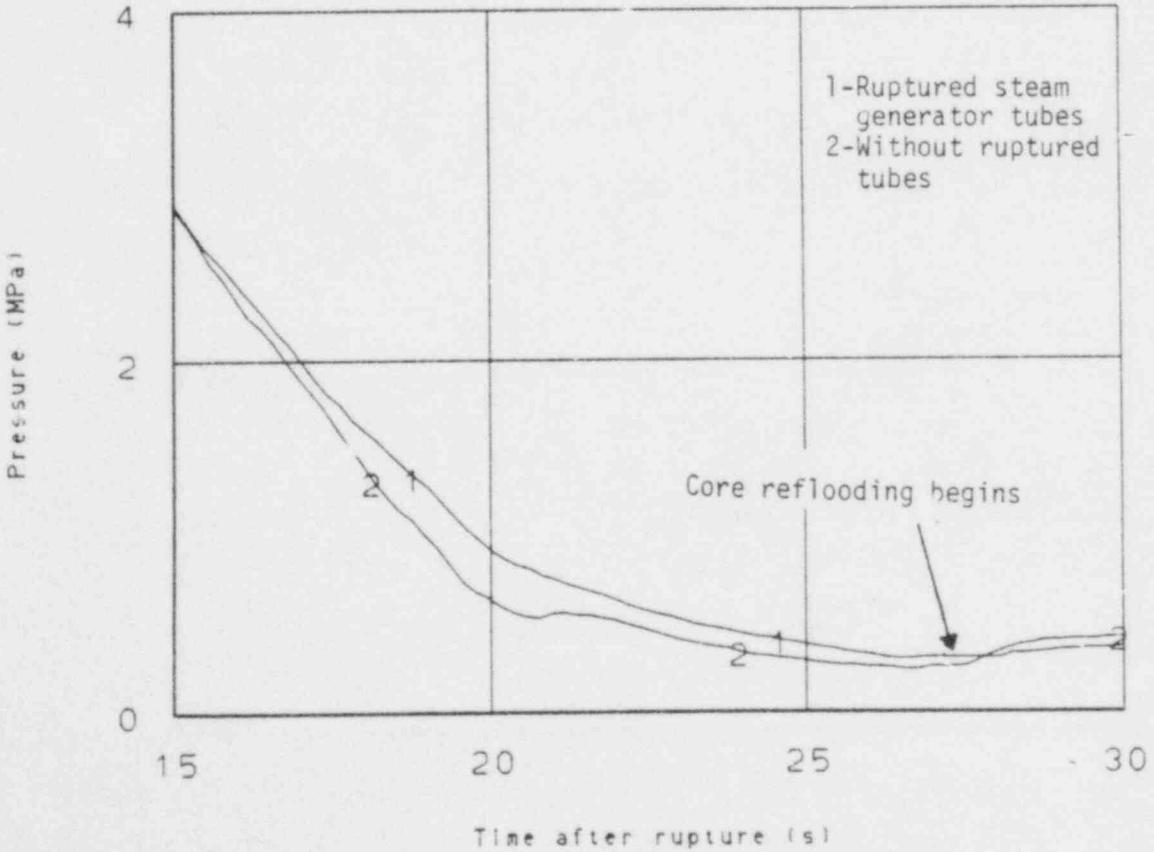


Figure 7. Pressure in cell 15 of the upper plenum adjacent to the loop 2 hot leg piping junction with and without the small rupture (15-30 s).

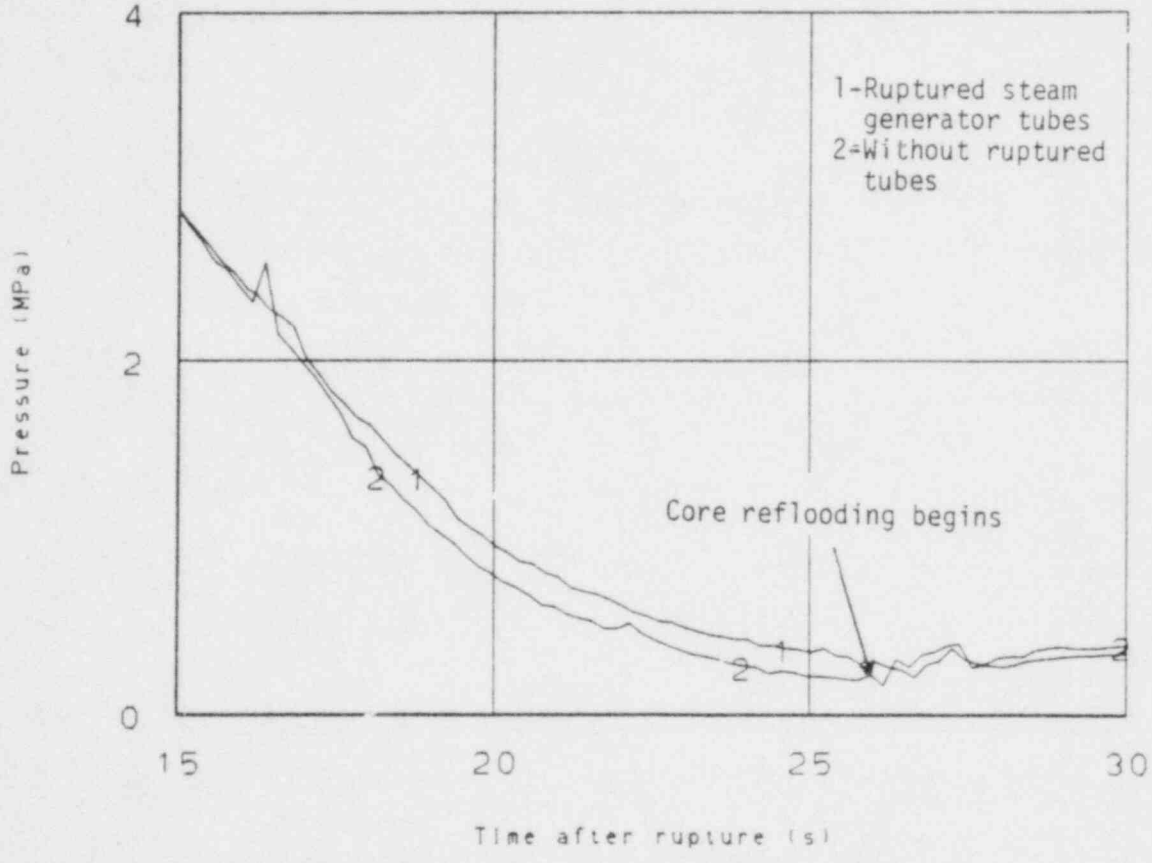


Figure 8. Pressure in cell 24 of the downcomer adjacent to the loop 2 cold leg piping junction with and without the small rupture (15-30 s).

Figures 9 and 10 show the downcomer and lower plenum liquid volume fractions during the first 30 s of the transient for the calculations with and without the small rupture. The lower plenum lost considerable liquid during the initial core flow reversal (core inlet mass flow rate is shown in Figure 11). As the pressure gradient across the core began to equalize, the core flow returned to a normal positive direction. The liquid contained in the downcomer fell back to the lower plenum. For the calculation without ruptured steam generator tubes, slightly more mass from the intact loops entered the downcomer at about 5 s (Figure < is representative of all intact loops) resulting in somewhat more mass in the downcomer and lower plenum after 5 s than for the calculation with the small rupture.

After peaking at about 7 s the downcomer continued losing mass with most of the liquid entering from the intact loops carried out the broken loop (loop 1) cold leg break. At about 13 s the accumulator injection began to replenish the liquid in the downcomer but the liquid did not enter the lower plenum until the pressurizer was nearly mass depleted permitting the flow in loop 4 to return to its normal pattern at about 17 s. The mass leaving the pressurizer after 17 s was swept through the loop into the downcomer.

At about 18 s the flow into the downcomer was larger for the small rupture calculation than for the calculation without rupture but the liquid was carried out the cold leg break instead of traveling to the lower plenum, Figure 12.

After 20 s, corresponding to the blockage of normal flow in loop 2, the differences in downcomer and lower plenum behavior became pronounced. The downcomer filled with liquid for the calculation without ruptured steam generator tubes because of slightly more flow into the downcomer and slightly less flow out the break than for the small rupture calculation. At 23 s the pressure difference between the downcomer and containment diminished for the calculation without rupture and the cold leg break flow

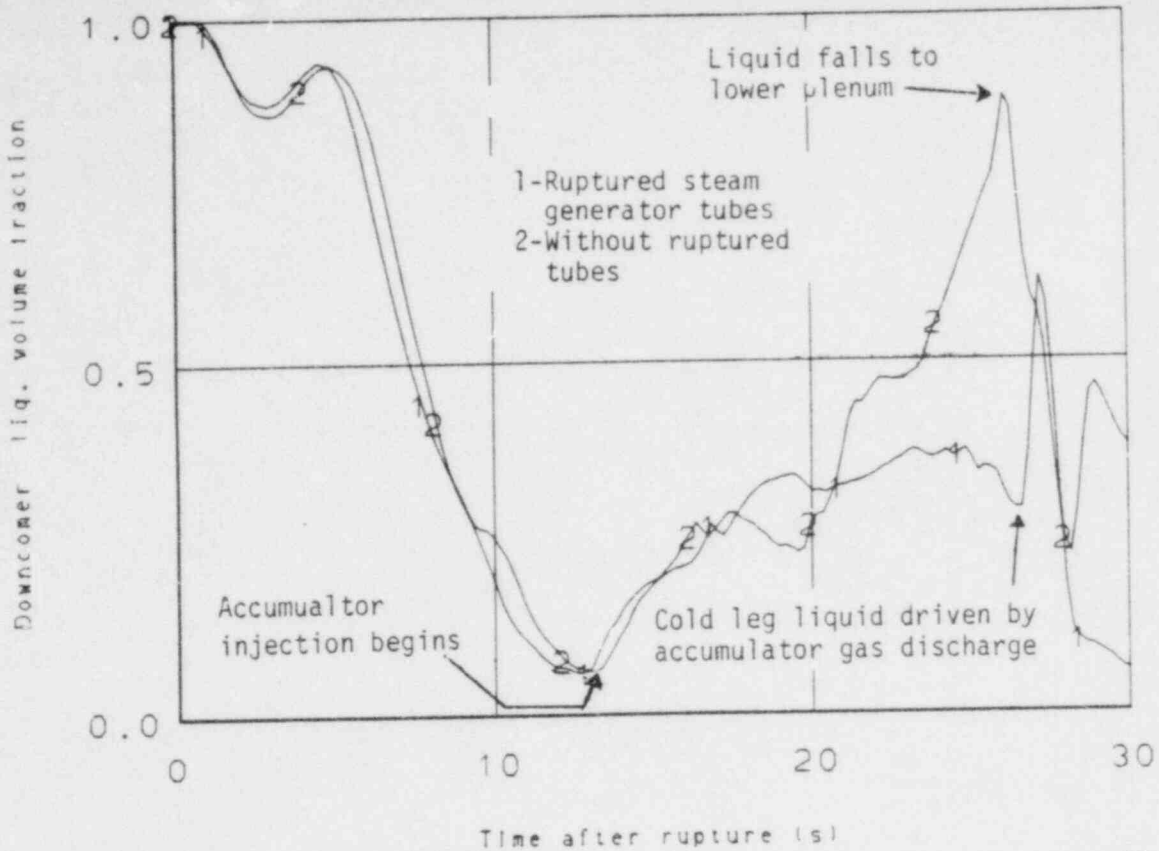


Figure 9. Downcomer liquid volume fraction with and without the small rupture (0-30 s).

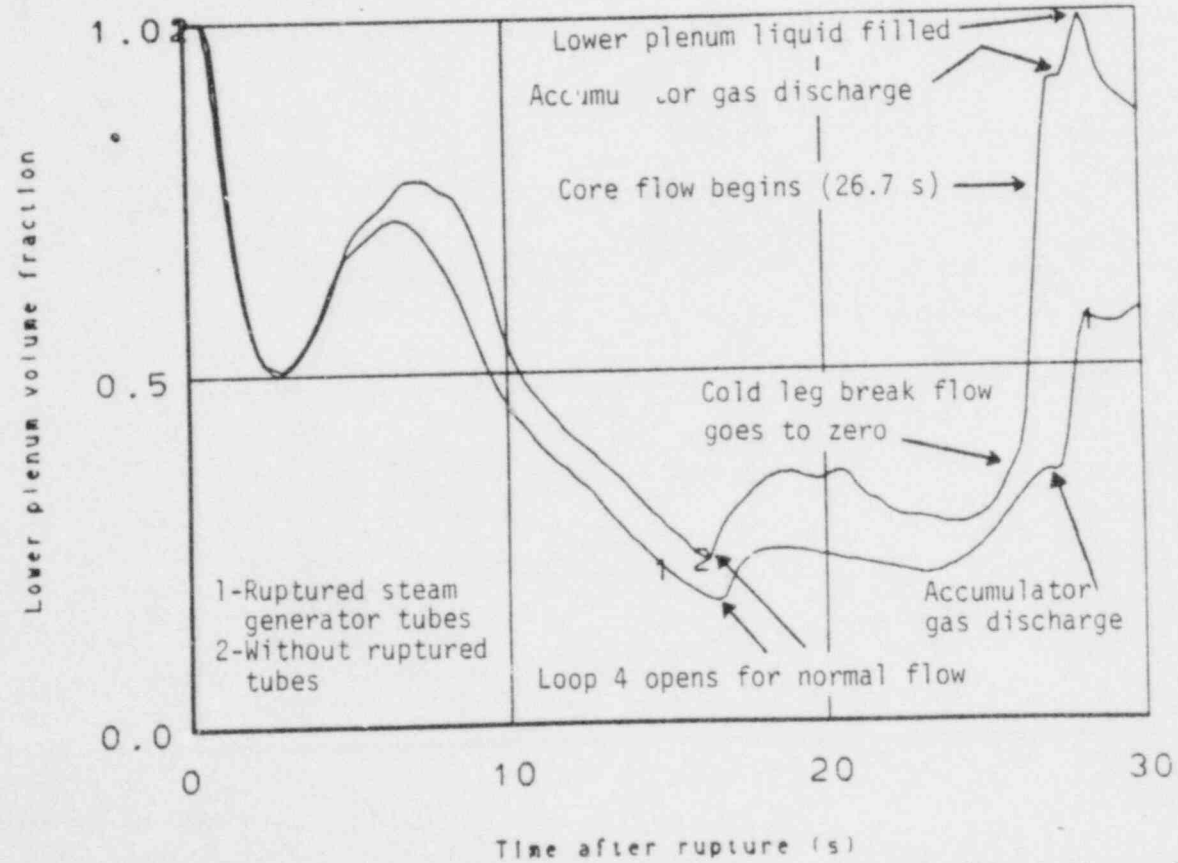


Figure 10. Lower plenum liquid volume fraction with and without the small rupture (0-30 s).

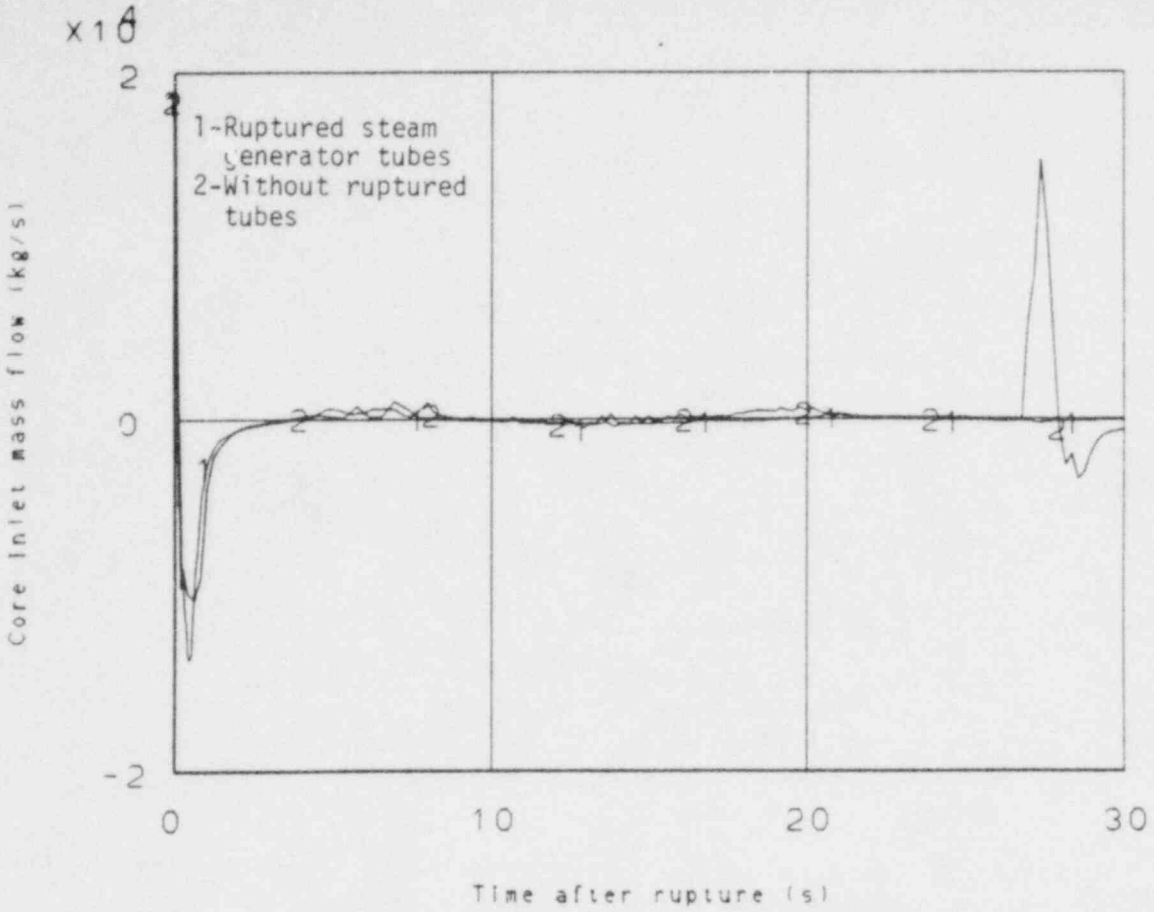


Figure 11. Core inlet mass flow rate with and without the small rupture (0-30 s).

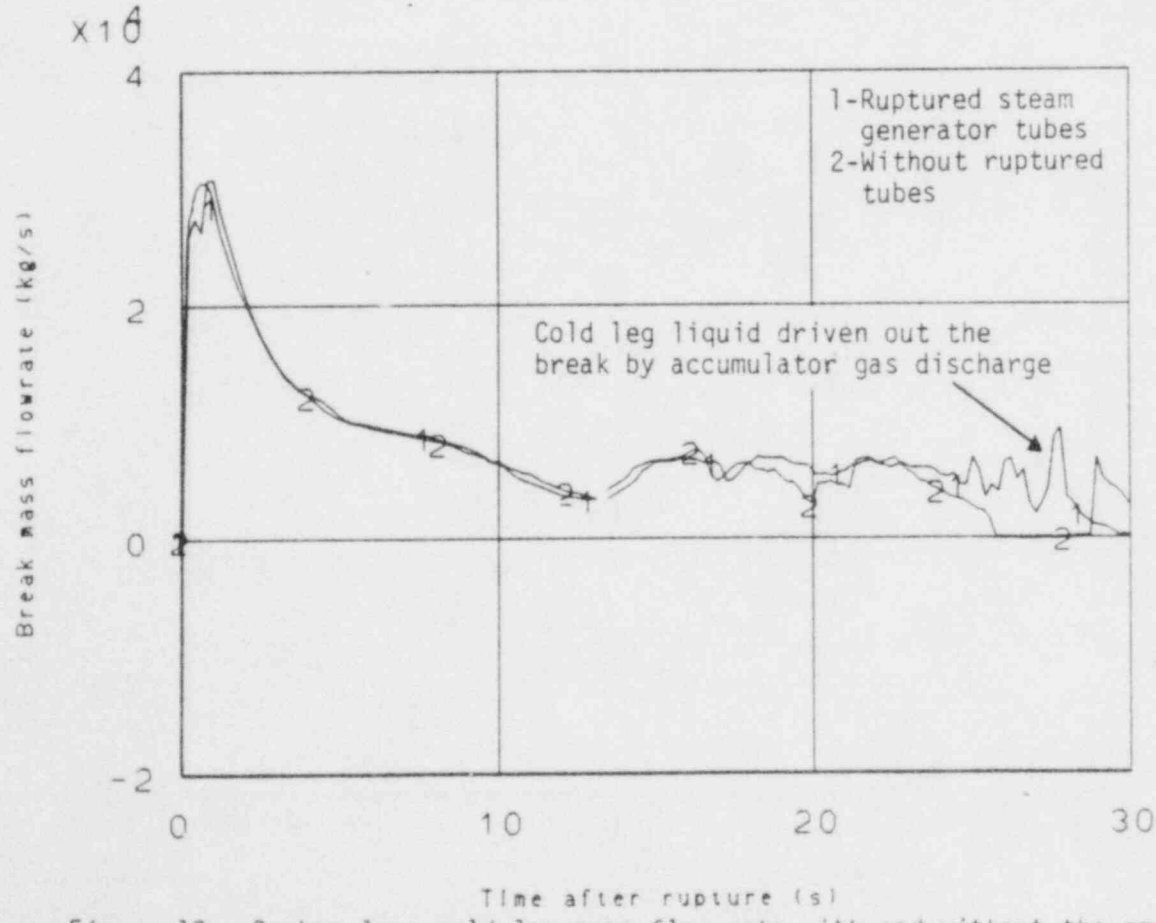


Figure 12. Broken loop cold leg mass flow rate with and without the small rupture (0-30 s).

also diminished, Figure 12. For the small rupture calculation the flow from the rupture to the upper plenum kept the entire system at a higher pressure. Thus upward flow continued through the downcomer entraining and carrying liquid supplied by the ECC systems out the break.

At about 25.8 s for the calculation without rupture the cold leg break flow rate dropped to zero or reversed slightly. The liquid in the downcomer dropped quickly almost filling the lower plenum liquid full, Figure 10. The rapid filling of the lower plenum raised a two phase mixture up into the core, Figure 11.

For the small rupture calculation, the liquid inventory in the downcomer did not change sharply until the large volumetric gas flow rate from the accumulators forced liquid from the intact cold leg piping into the downcomer. A portion of this liquid was forced out the cold leg break and a portion fell into the lower plenum but not in sufficient volume to refill the lower plenum, Figure 12 .

The short term hot leg break mass flow rate is shown in Figure 13. It was essentially the same for both calculations.

In summary, the mass flow entering the primary system from the ruptured steam generator resulted in increased steam flow up the downcomer which retarded lower plenum refill when compared to the calculation without rupture.

### 3.1.2 Small Rupture Long Term Results (30-150 s)

With the end of accumulator injection, the reflooding process had begun for the calculation without ruptured steam generator tubes.[2] However, for the calculation with a small rupture, the lower plenum was roughly only 60% full of liquid at 30 s when the accumulators were empty. Fluid was being furnished to the system from the ECC systems in the intact loops and from the ruptured steam generator secondary side. About 210 kg/s

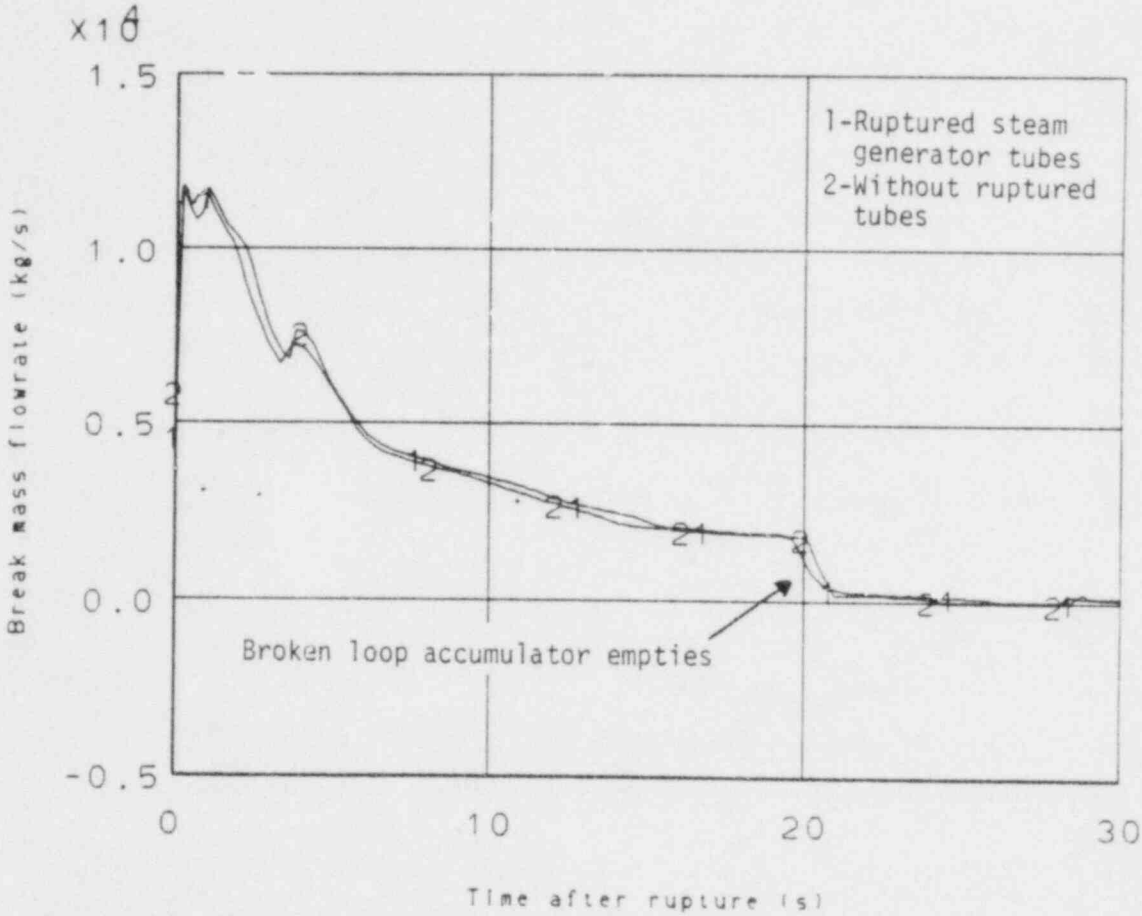


Figure 13. Broken loop hot leg mass flow rate with and without the small rupture (0-30 s).

of this fluid reached the lower plenum, the remainder flowed out the breaks. Refill was completed at about 92.7 s.

Figure 14 shows the lower plenum and downcomer liquid volume fraction change as the lower plenum filled. Figure 15 shows the break mass flow rates and Figure 16 shows the mass flow rates exiting the ruptured steam generator tubes and entering the vessel upper plenum and downcomer, respectively, from loop 2 containing the ruptured steam generator.

During the time period between the termination of accumulator injection and the completion of refill, a homogeneous mixture of liquid and vapor (quality of approximately 0.2) entered the upper plenum from loop 2 containing the ruptured steam generator tubes. The phases separated with the liquid falling into the core. The radial momentum of the fluid carried most of the liquid preferentially through cell 15 of the outer vessel ring to cell 7 of the inner vessel ring of vessel level 10 where it dropped into the core. Some liquid stayed in cell 15 and some passed through cell 7 to cells 6 and 8 also of the inner ring. With a different type of cell arrangement the radial momentum would have likely carried the liquid across the upper plenum to the opposite wall.

Figure 17 shows the liquid velocities at the cell interfaces of level 10, the level connected to the hot leg piping. Also shown in Figure 17 are the cell average void fractions. The specific time selected (81.2 s) was representative of the values during the time period being considered. The void fraction of the fluid in cell 7 was less than that of the fluid entering the upper plenum (0.966 compared to 0.992) indicating a storage of liquid. (A small change in void fraction changes the mixture density significantly at the pressures being considered). Void fractions in cells 6, 8 and 15 were slightly more. Figure 18 shows the same quantities for level 9, and the vapor velocities are also shown. The axial velocities associated with level 9 are at the interface between level 9 and 10 and thus indicate whether the fluid was moving into or out of the core.

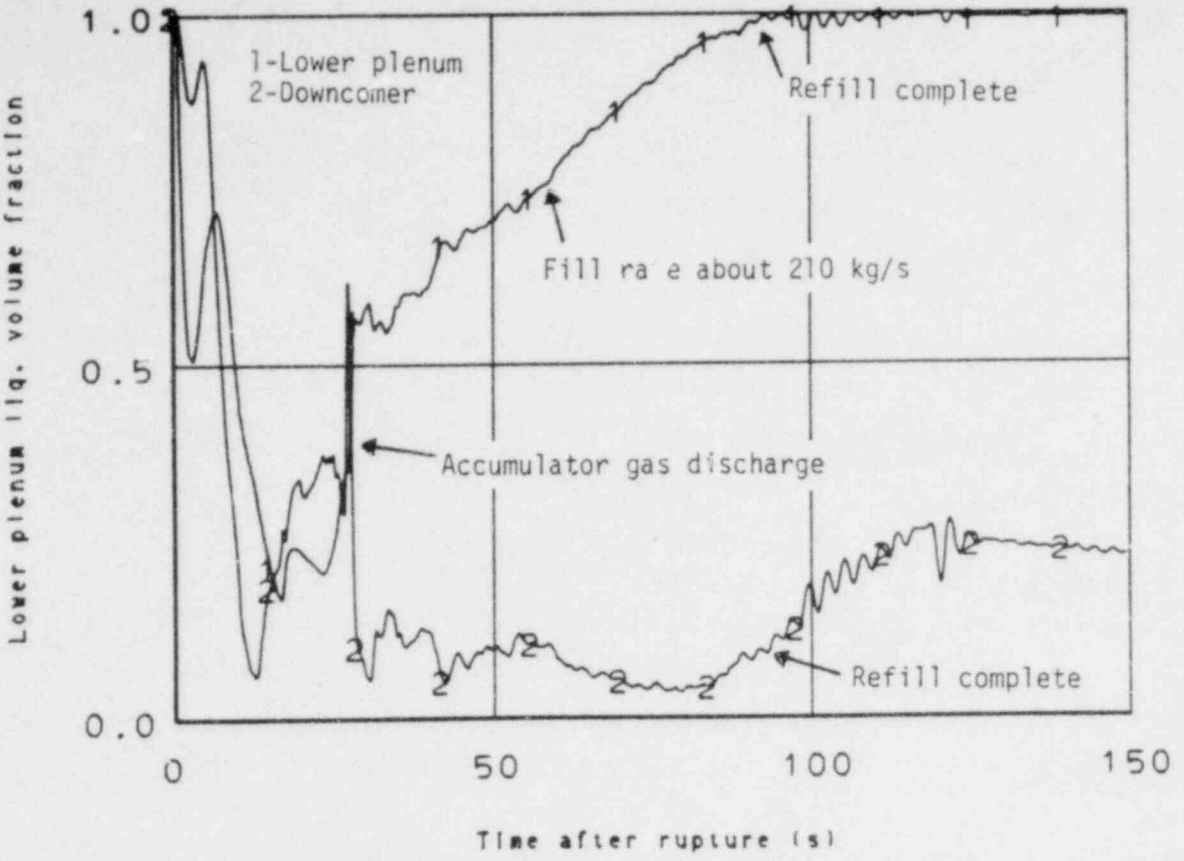


Figure 14. Lower plenum and downcomer liquid volume fractions during the small rupture.

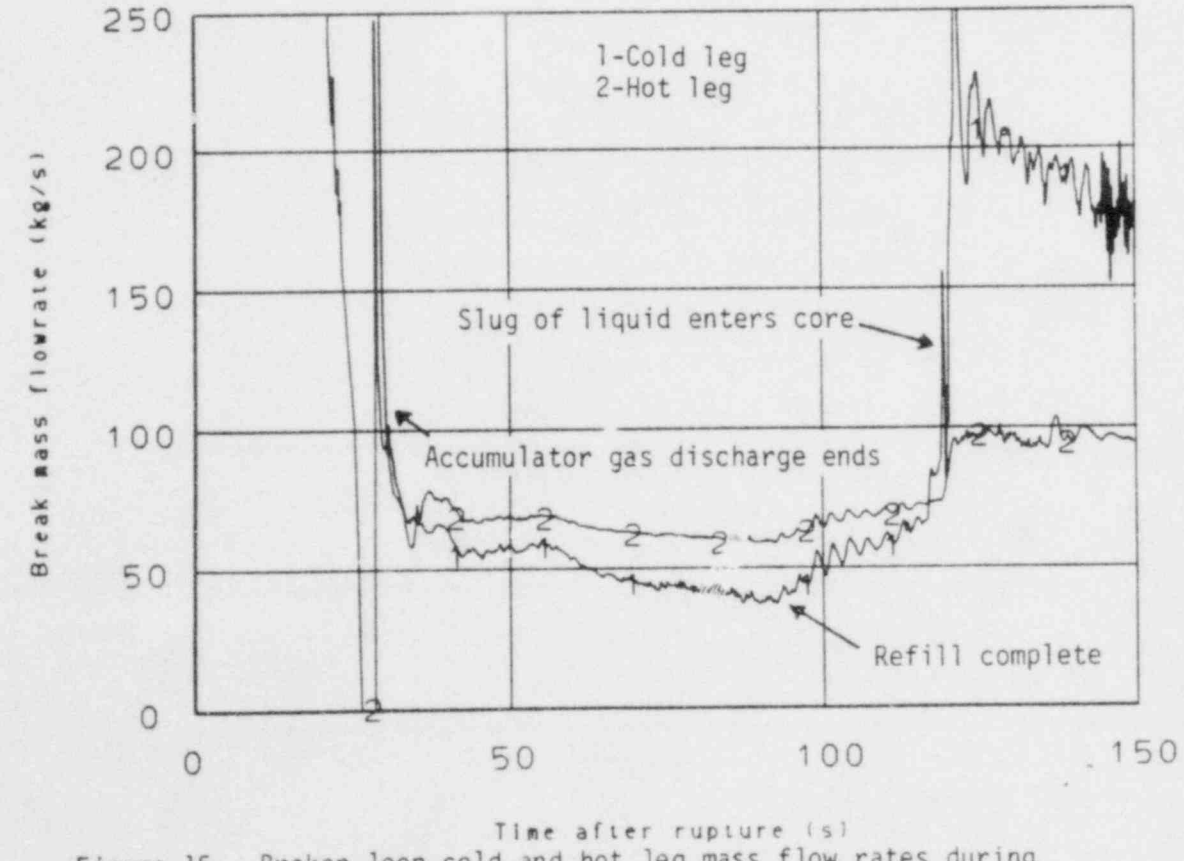


Figure 15. Broken loop cold and hot leg mass flow rates during the small rupture.

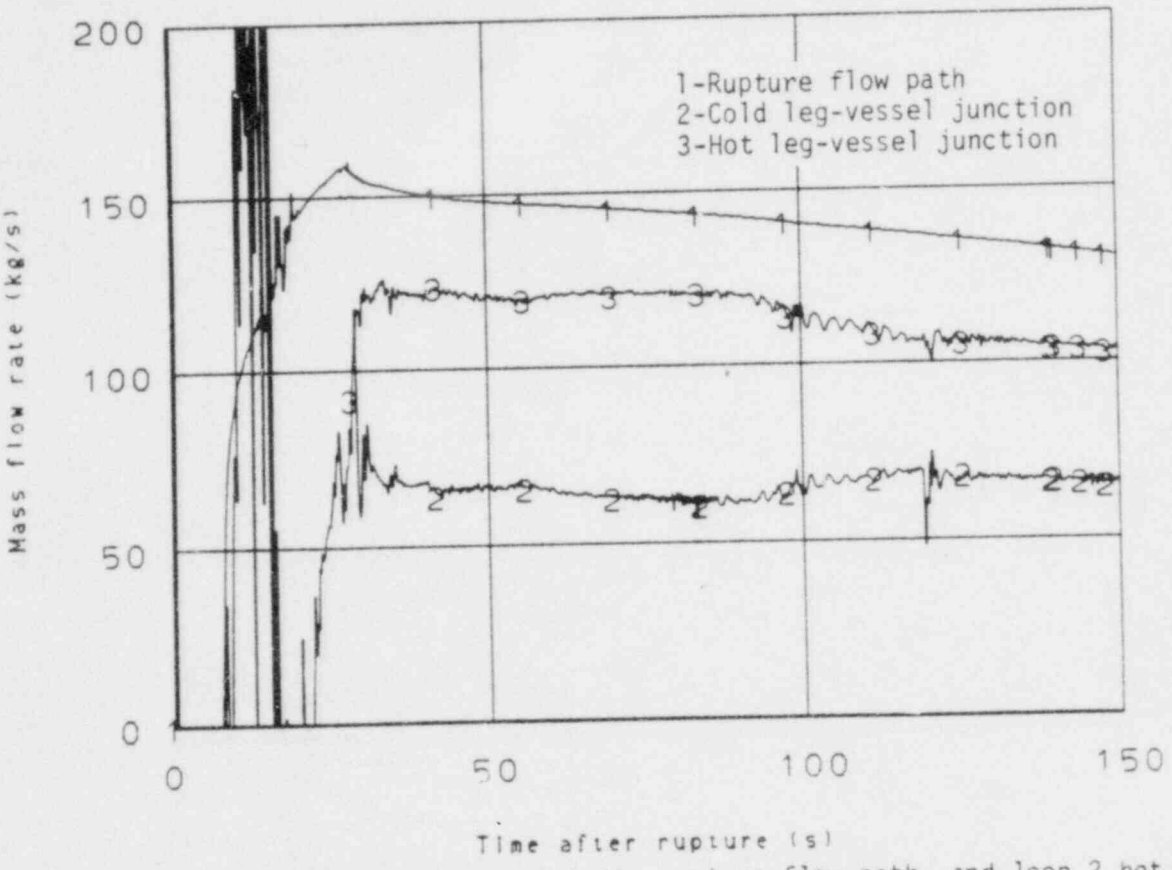


Figure 16. Mass flow rates through the rupture flow path, and loop 2 hot and cold leg vessel junctions during the small rupture.

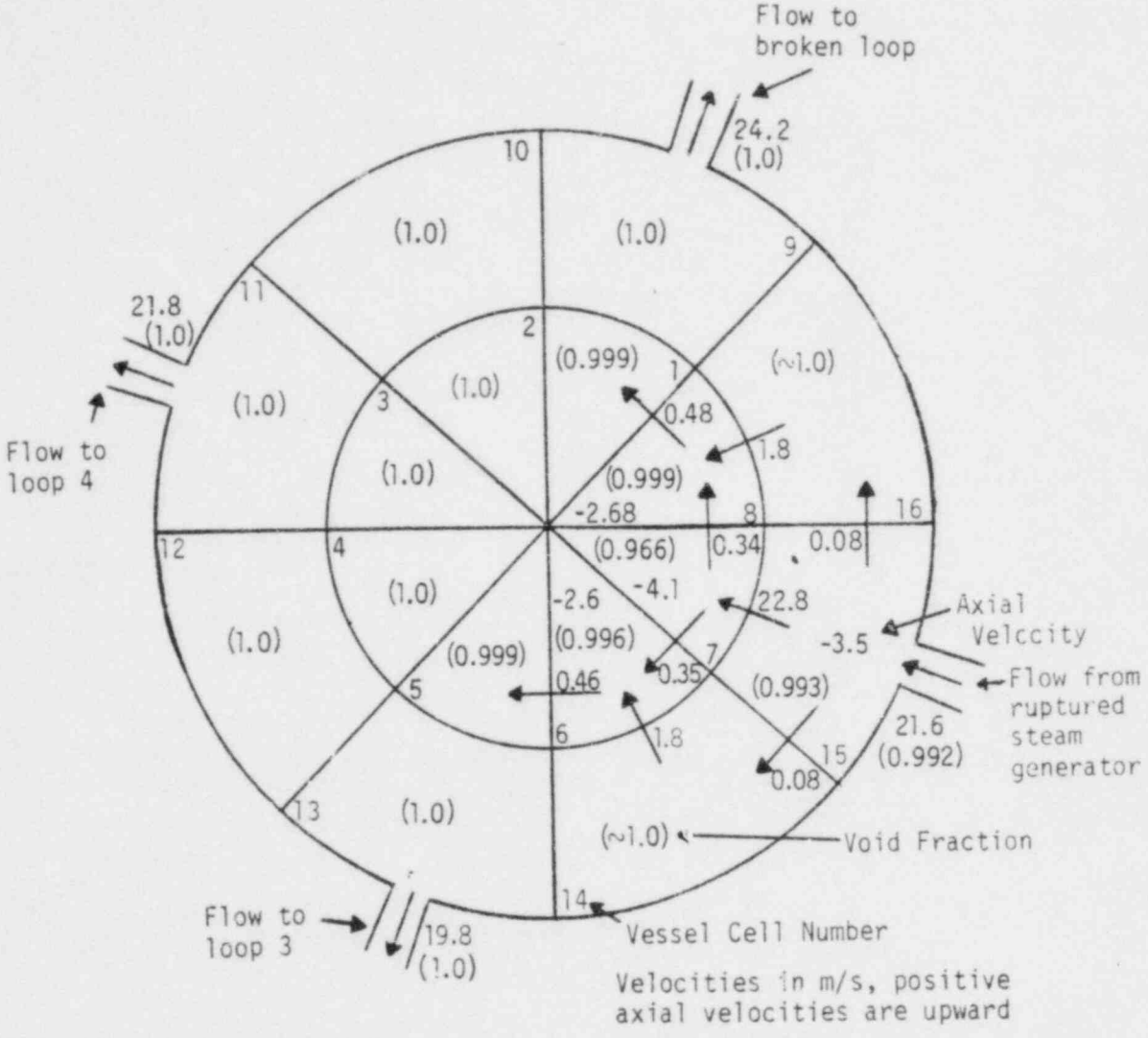


Figure 17. Axial, radial, and tangential liquid velocities and cell void fractions in vessel level 10 at 81.2 s.

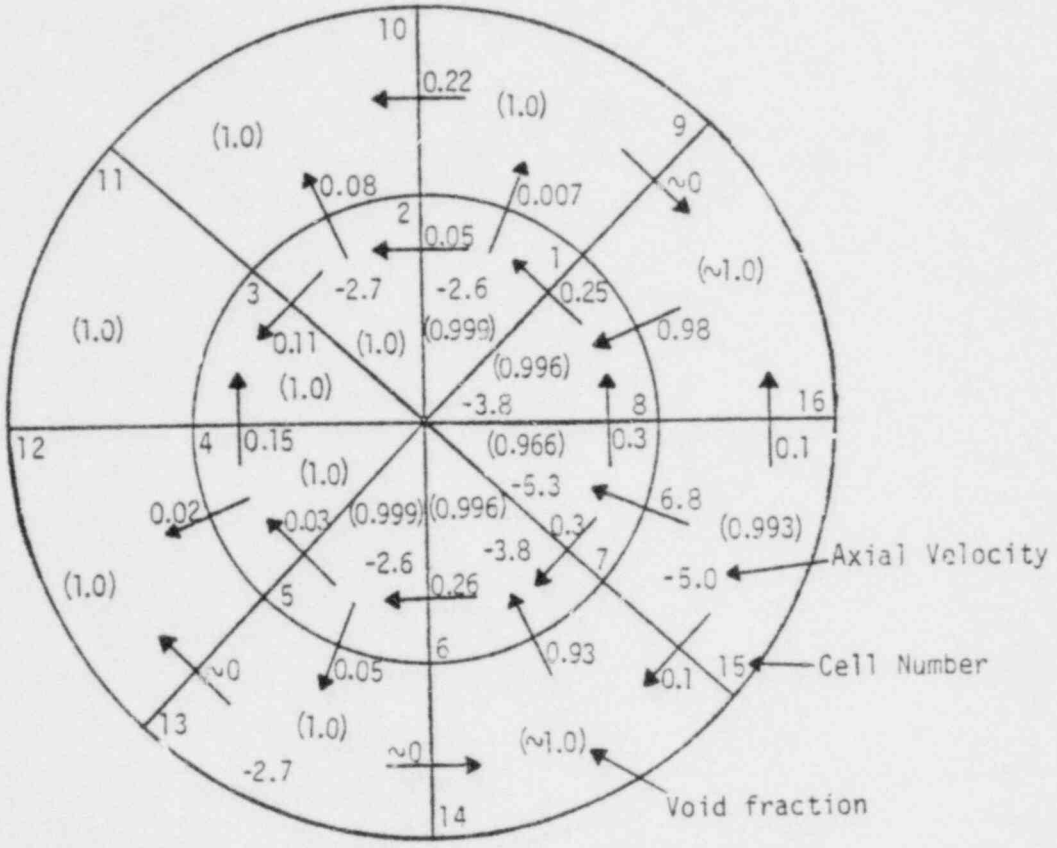


Liquid velocities in m/s, positive axial velocities are upward

Figure 18a. Liquid velocities and cell void fractions in vessel level 9 at 81.2 s during the small break.

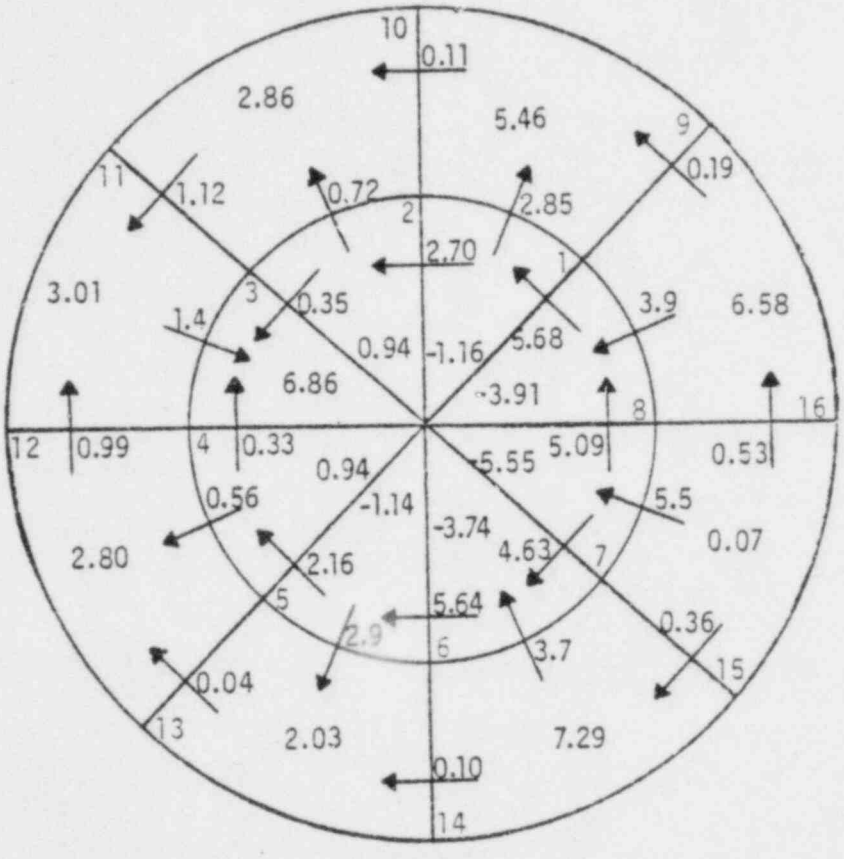


Vapor velocities in m/s, positive axial velocities are upward

Figure 18b. Vapor velocities in vessel level 9 at 81.2 s during the small rupture.

Figure 17 shows that while the liquid is being distributed across the upper plenum it tends to remain in cells 6, 7, 8 and 15. In cell 5 counter-clockwise through 1 the vapor moves downward with the liquid while in the remaining cells the vapor moves upward. Further examination of the void fractions, and vapor and liquid velocities in the core indicated that a small amount of liquid was distributed throughout the core but that it remained predominately in cell 7. In the upper half of the core the vapor generated by evaporation of the liquid from the ruptured steam generator flowed upward whereas in the two lower core levels the vapor flowed downward with the remaining liquid and entered the lower plenum.

During this time interval about 120 kg/s of two phase fluid entered the upper plenum from the ruptured steam generator tubes. About 60 kg/s of vapor exited the hot leg break and about 20 kg/s of vapor entered each of the remaining intact looo hot legs. Therefore about 20 kg/s of a two phase mixture reached the lower plenum directly from the upper plenum.

The effect of the fluid channeling in cell 7 is further illustrated in Figure 19 which shows the cladding surface temperatures of the bottom and top core levels for the fuel rods located in vessel cells 2 and 7. The additional cooling provided to cell 7 resulted in considerably lower cladding temperatures. The rods of cell 2 were selected because they are in the inner core ring, are relatively unaffected by the flow through the core from the rupture, and exhibit the highest cladding temperatures. The core top and bottom level temperatures are shown because they represent the most realistic values obtained. The code computed gap conductance was unrealistically small, thus the rods initially contained too much stored energy and subsequently the core midplane cladding temperatures during the transient were not representative of expected results. The effect was minimized for the top and bottom levels. The magnitude of the excess cladding temperatures was determined in Reference 2 to be about 130 K for the top and bottom core levels at 40 s for the calculation without ruptured steam generator tubes.

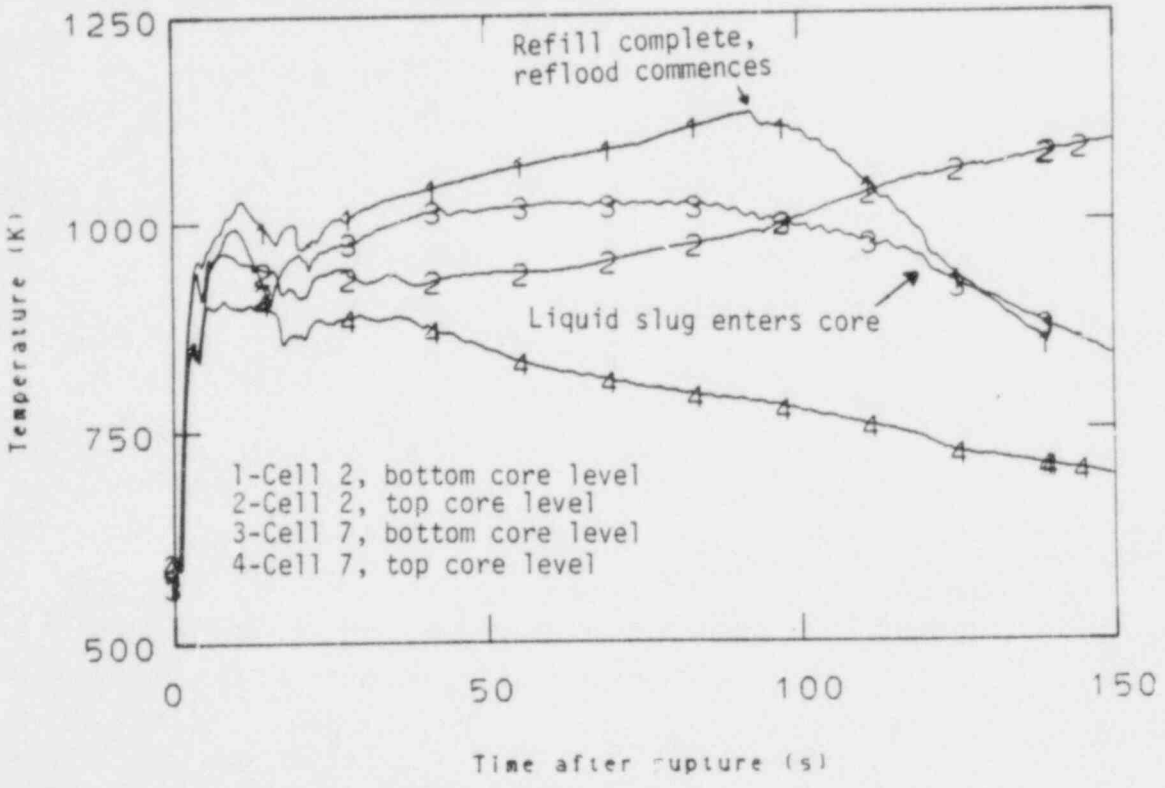


Figure 19. Cladding surface temperatures for top and bottom core levels of cells 1, 2 and 7 during the small rupture.

With the completion of lower plenum refill (see Figure 14) at about 93 s, the additional vapor generation in the core lower level caused by liquid entering the core increased the system pressure and resulted in increased break flow rates as shown in Figure 15. Figure 19 shows the effect on the cladding temperature in vessel cell 2. The cladding temperature of the bottom level turned around whereas the cladding temperature of the top level was not affected. The effect of reflooding on the cladding temperatures in cell 7 was not significant, apparently due to the good cooling already being obtained from the preferential flow of liquid furnished by the ruptured stream generator.

With the onset of bottom flooding the core began to refill with liquid (see Figure 20) and a bottom quench front was established. At about 119 s the downcomer liquid head was sufficient to push a slug of liquid into the lower level of the core. A large volume of vapor was consequently generated which increased the system pressure and forced additional mass out the broken loop (see Figure 15). The quench from the bottom continued as shown in Figure 21 (about 0.08 m in 50 s). The cooling of the top level of the core in cells 6, 7 and 8 was sufficient to promote a falling film quench front as shown in Figure 22. The falling film quench position for cell 7 was moving rapidly.

At this time the rise in the peak midplane cladding temperatures had been arrested and quenching of the core from both ends had commenced. The ruptured steam generator would have continued to supply fluid to the system for about 200 more seconds. It appears that the quenching process would continue to completion. Because of the slow quench process it was decided to terminate the calculation. Complete quenching could have taken several hundred more seconds. The time required to run this calculation on the Control Data Corporation 176 computer was 16.1 hours. The computation rate was about 12.4 s per hour at termination.

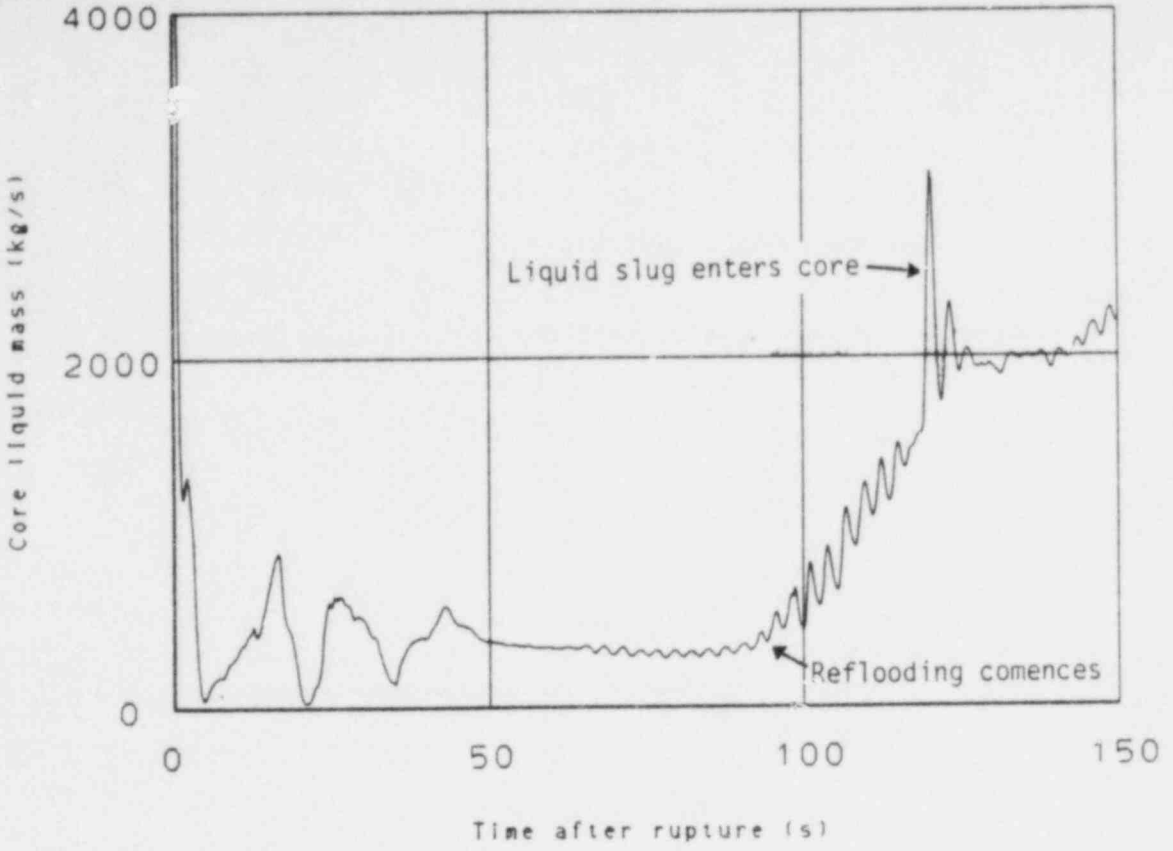


Figure 20. Core liquid mass inventory during the small rupture.

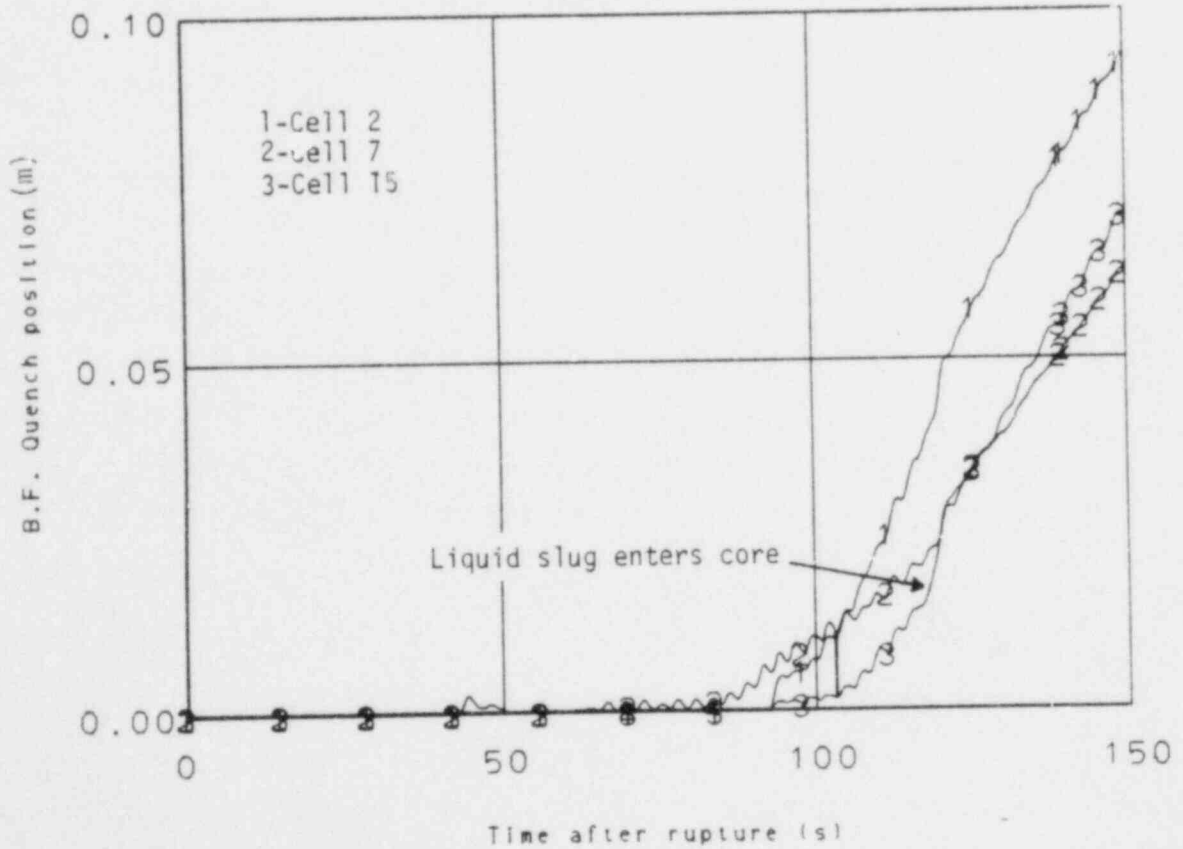


Figure 21. Bottom flooding quench position on rods in cells 2, 7 and 15 during the small rupture.

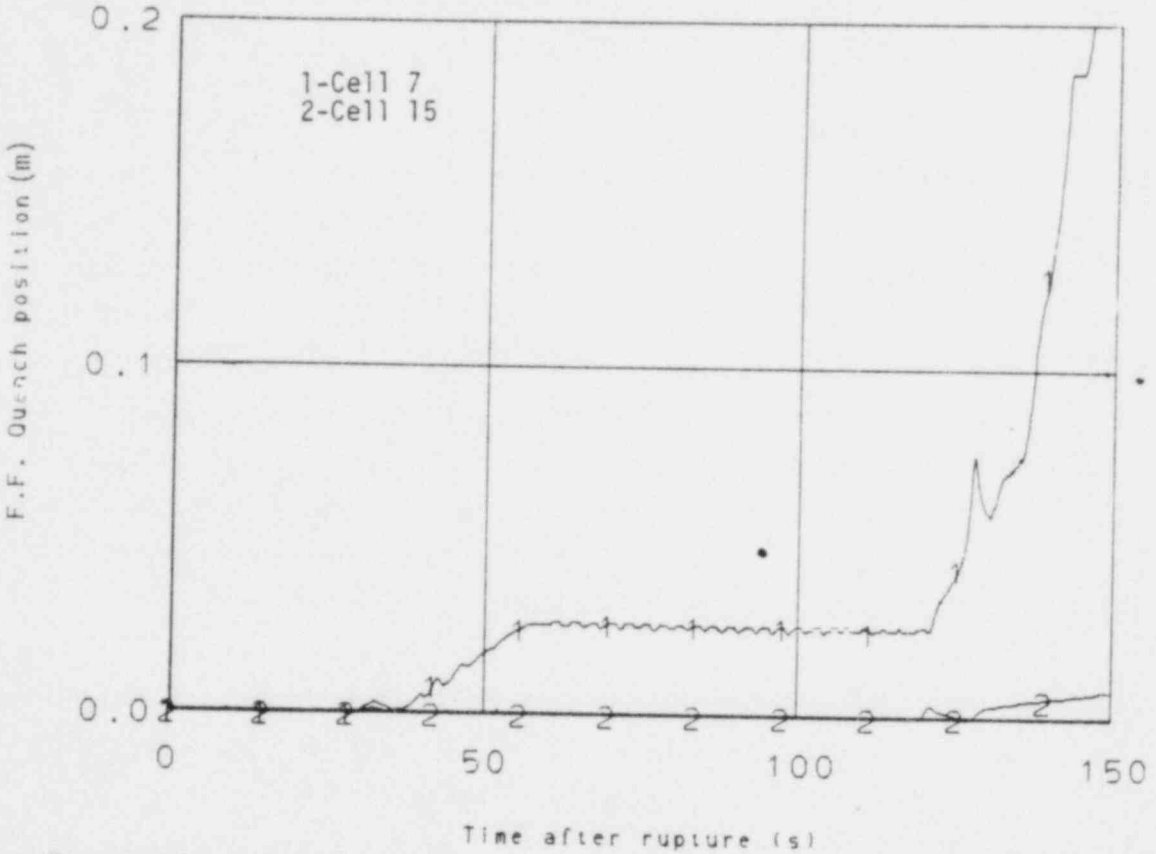


Figure 22. Falling film quench position on rods in cells 7 and 15 during the small rupture.

## 3.2 Large Rupture

During the early portion of the transient (0-30 s) the calculated behavior of the PWR with a large number of ruptured steam generator tubes was approximately the same as that of the same system exposed to a small rupture. Beyond 30 s the calculated phenomena differed significantly. Thus, the following discussion is broken into short term and the longer term results. Comparisons are made with the small rupture calculation where appropriate.

### 3.2.1 Large Rupture Short Term Results (0-30 s)

The differences between the calculated phenomena for the small rupture and large rupture are relatively minor during the early portion of the transient. The pressurizer and accumulator responded in the same way as shown for the small break and the flow patterns throughout the system were also very similar. About 4 times more flow entered the system from the large rupture than for the small rupture after the system pressure dropped below the pressure of the steam generator secondary side. Because of this larger flow rate from the steam generator rupture, the mass flow into the upper plenum was also much larger and blockage of loop 2 to normal flow occurred about 12 s instead of at 20 s as occurred for the rupture of a small number of steam generator tubes.

As a result of the slightly earlier blockage of loop 2 and slightly higher upper plenum pressure, less liquid from the downcomer dropped into the lower plenum for the large rupture calculation than for the small rupture calculation. (About 2000 kg less liquid was in the lower plenum after accumulator injection ended for the large rupture as compared to the small rupture calculation.) Figure 23 shows a comparison of the lower plenum liquid volume fraction for the small and large ruptures. The cladding temperatures were about 10-20 K lower at this time for the large rupture than for the small rupture calculation. Thus at the end of accumulator injection the lower plenum was far from being refilled.

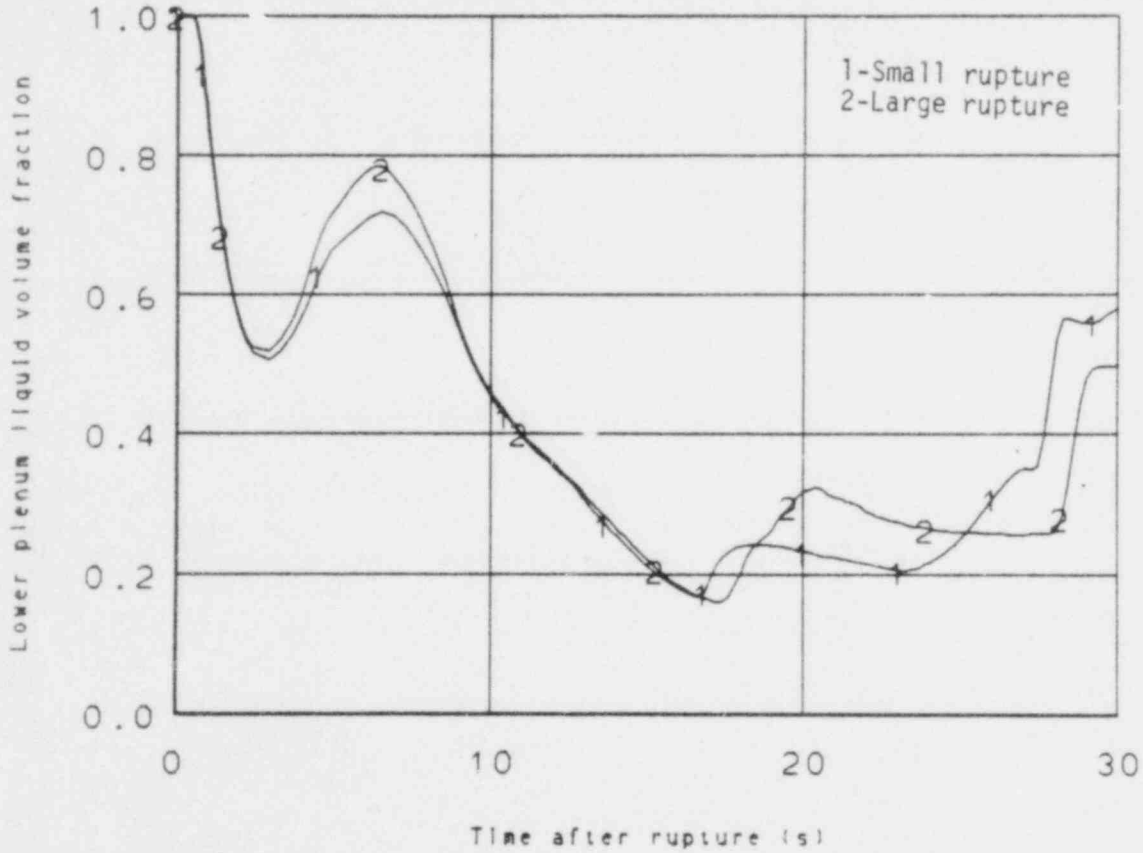


Figure 23. Lower plenum liquid volume fraction for the small and large ruptures during the first 30 s of the transient.

However, better cooling was occurring because of the increased fluid entering the upper plenum from the ruptured steam generator.

### 3.2.2 Large Rupture Long Term Results (30-150 s)

Figure 24 shows the mass flow rate through the ruptured steam generator tubes connecting the primary and secondary sides of the steam generator. Also shown are the mass flow rates leaving loop 2 and entering the upper plenum and downcomer. The rupture flow rate reached a near constant value of about 800 kg/s at 25 s and remained nearly constant to about 39 s. At 40 s the flow rate was at the scaled value of 600 kg/s. The reservoir of fluid in the secondary side was not sufficient to maintain a constant flow rate through the large rupture as was the case for the small rupture. Consequently the rupture flow rate, and hot and cold leg flow rates diminished with time. At about 96 s (when 230 kg/s were entering the upper plenum) the behavior of the system changed as will be discussed in the following text.

The liquid entering the upper plenum from loop 2 flowed preferentially across vessel cell 15 to cell 7 as it did for the small rupture discussed previously. The liquid penetrated the core to the lower plenum in sufficient magnitude to develop a pronounced falling film quench front on the rods in cell 7. Some of the liquid entering the upper plenum scattered across the core and falling film quench fronts were initiated in other vessel cells also.

The effect of the rupture flow on the core is illustrated in Figures 25, 26 and 27. Figure 25 shows the cladding temperature of the top and bottom core levels for vessel cells 2 and 7. The rod temperatures in cell 7 were significantly lower than for the rods in cell 2. Also the top level of cell 7 experienced quenching because of the falling film. Figure 26 shows the progression of the falling film on the rods of cell 7 and several other cells. Figure 27 shows the quench front on the bottom of the rods in cell 7. This quenching was caused by liquid falling through

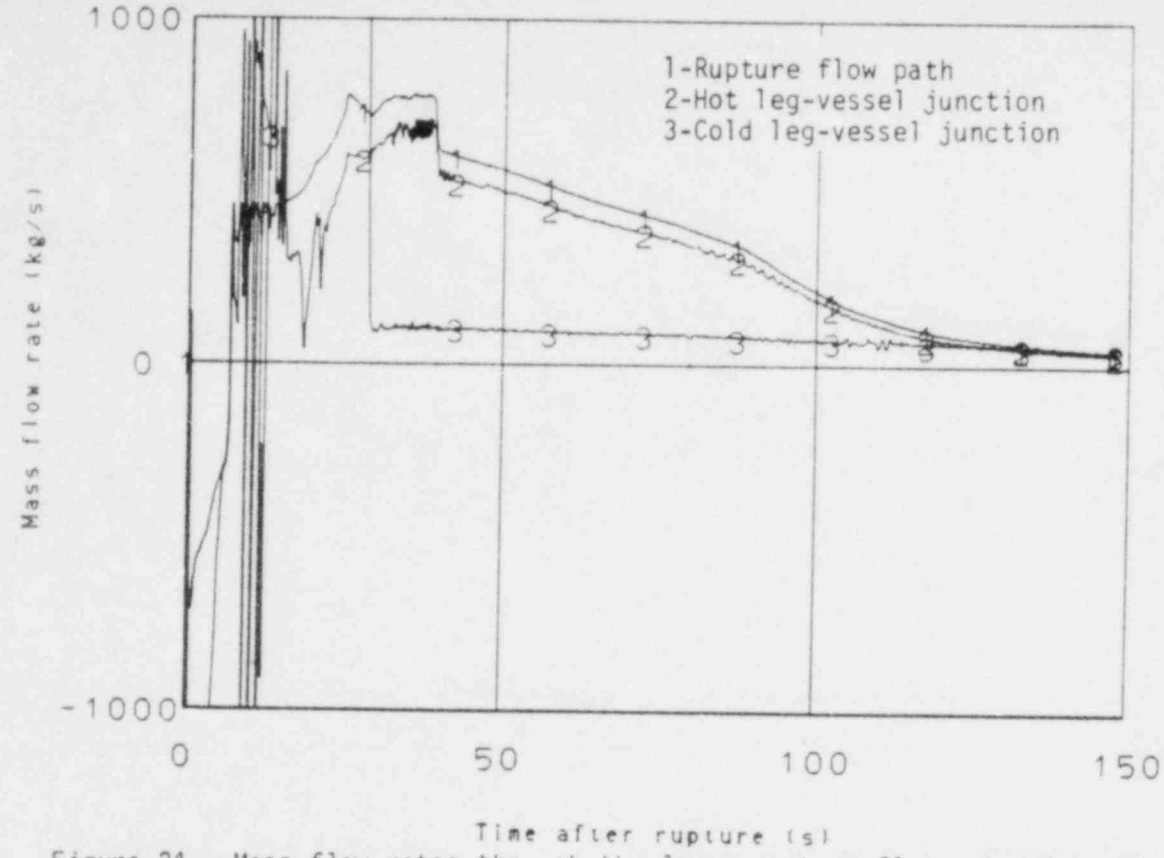


Figure 24. Mass flow rates through the large rupture flow path and the loop 2 cold and hot leg vessel junctions during the large rupture.

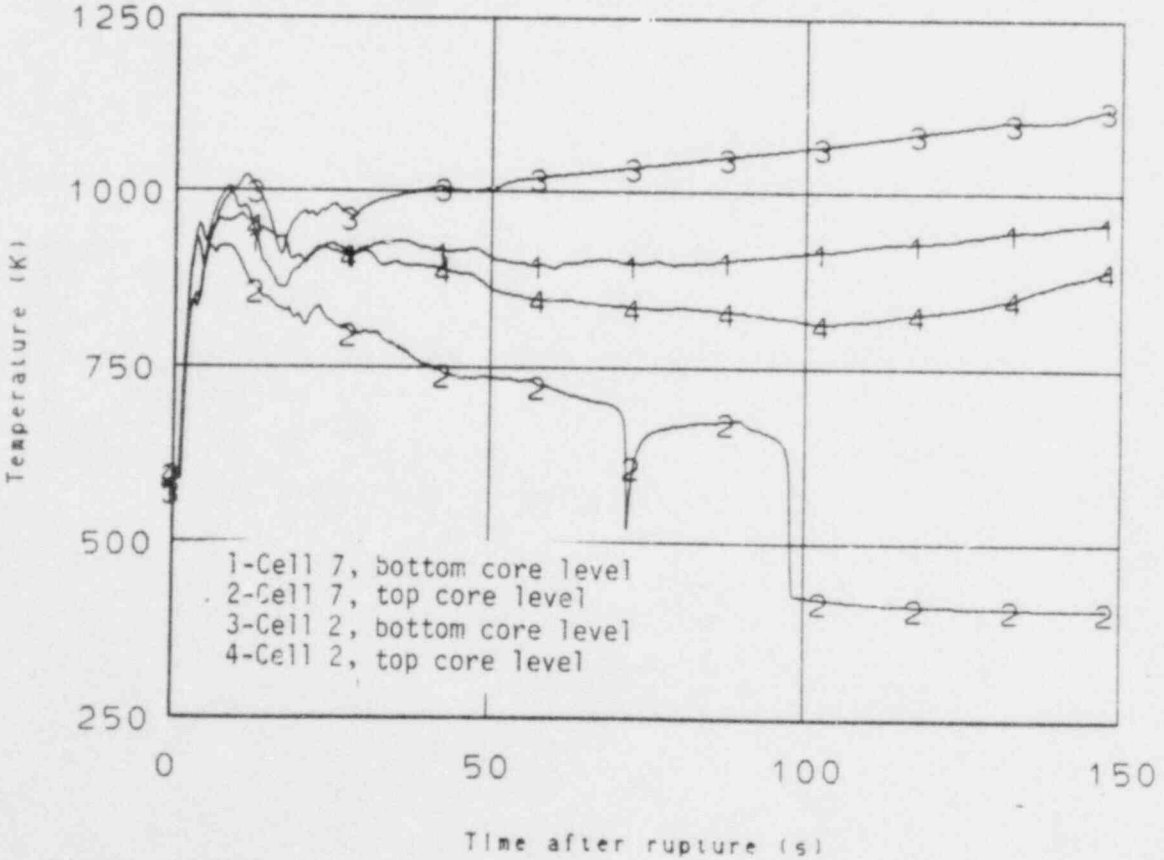


Figure 25. Cladding surface temperatures for top and bottom core levels of cells 2 and 7 during the large rupture.

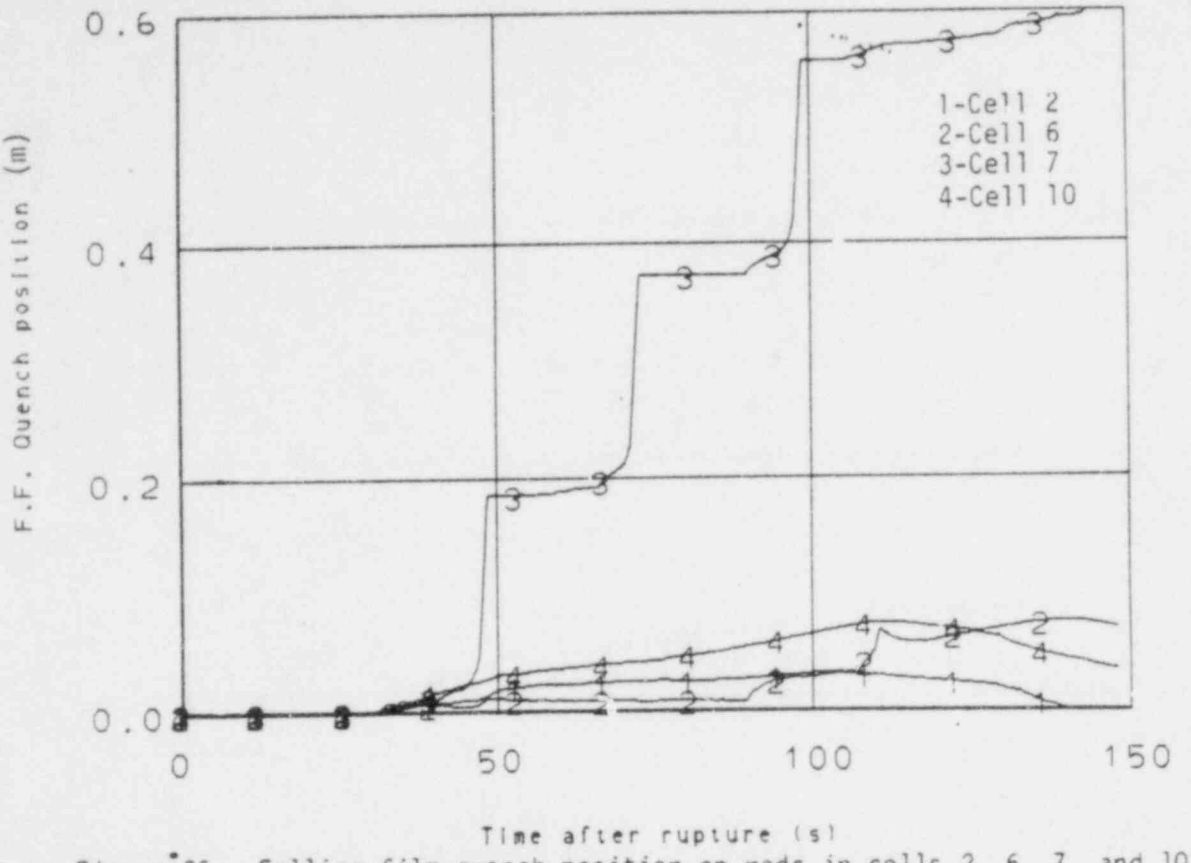


Figure 26. Falling film quench position on rods in cells 2, 6, 7, and 10 during the large rupture.

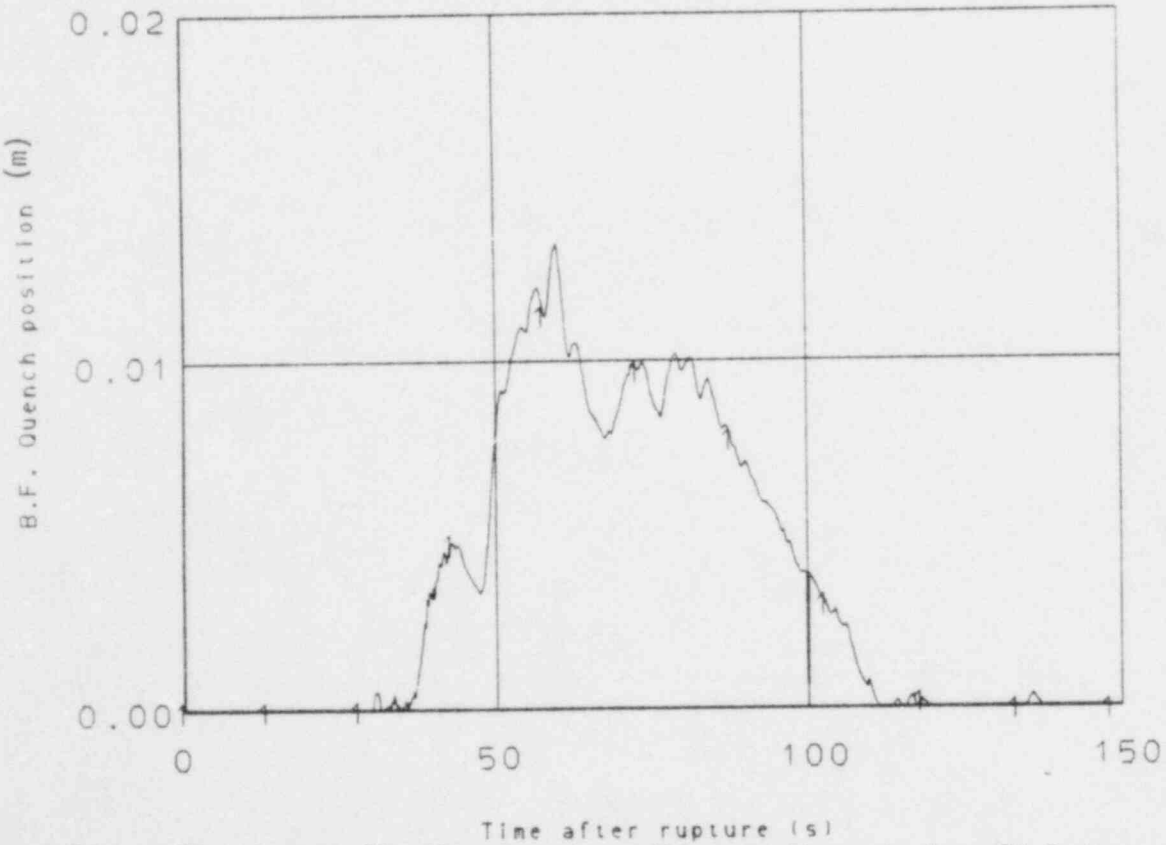


Figure 27. Bottom flooding quench position on the rods in cell 7 during the large rupture.

the core in sufficient quantity to rewet the low powered rod bottom. It does not appear likely that the midplane of cell 7 would have quenched even with the initial rod stored energy obtained with a more representative rod gap conductance.[2]

The quantity of fluid reaching the lower plenum from the rupture flow had an adverse effect on the liquid entering the downcomer from the intact loop cold legs and furnished by the safety injection systems. Vapor generated in the core in the lower levels flowed through the lower plenum into the downcomer. The upward vapor velocities in the downcomer were sufficient to keep liquid from accumulating in the downcomer and refilling the lower plenum. All the fluid entering the downcomer was swept out the broken loop cold leg until about 96 s (see Figure 28).

At 96 s the fluid quantity entering the upper plenum had diminished. The falling film quench positions on rods other than cell 7 were retreating. Also the bottom quench position on the rods in cell 7 was retreating. The cladding temperatures shown in Figure 25 increased at a slightly faster rate as the cooling of the core was consequently diminished.

Also, at 96 s the liquid entering the downcomer began to reach the lower plenum. The upward velocity at the bottom of the downcomer dropped to 2 m/s or less, permitting a small amount of liquid stored in the downcomer to move downward. At the time the calculation was terminated, the broken cold leg mass flow rate was approaching zero. The lower plenum was lacking about 6000 kg from being refilled. Assuming all of the safety injection coolant reached the lower plenum (approximately 120 kg/s) about 50 s would have elapsed prior to the commencement of bottom flooding. The elapsed computer time for the large rupture calculation was 23.3 hours. The computational rate was about 7.5 s per hour at termination.

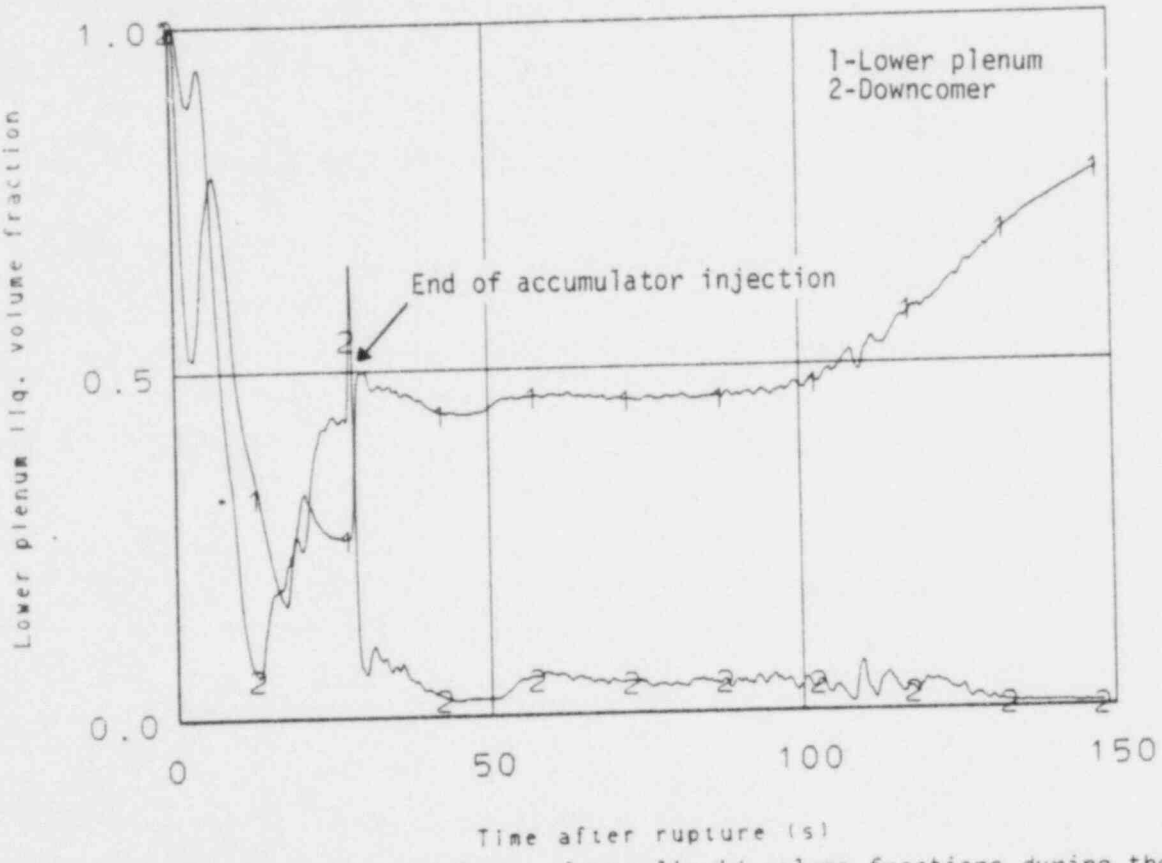


Figure 28. Downcomer and lower plenum liquid volume fractions during the large rupture.

## 3.3 Comparison With Semiscale Results

The effects of ruptured steam generator tubes were investigated experimentally and analytically by the Semiscale program.[4] The PWR calculations presented previously for small (approximate 16 ruptured tubes) and large (approximate 60 ruptured tubes) ruptures are compared below to experimental results obtained when rupture flow was initiated at the start of refill. The comparisons are made for the system hydraulic response and the core thermal response.

### 3.3.1 System Hydraulic Response

The emptying rate of the accumulators was significantly larger in the calculations than for the Semiscale Mod-1 system. (The discrepancy is attributed to the modeling technique applied to the accumulators as described in Appendix A). This resulted in different times for the beginning of refill and for the gas injection following accumulator liquid discharge. For example, refill commenced at about 6 s in the Semiscale Mod-1 system coincident with gas injection. Refill began at about 24 s in the calculation and gas injection occurred at about 27 s. These differences did not appear to affect the hydraulic behavior pattern significantly as the major effects are similar when the rupture flow was initiated at or prior to refill. Delay in rupture flow until after refill but before reflooding would result in a larger liquid inventory in the downcomer and lower plenum. As the inventory increased, the time of reflooding would have been earlier and the maximum temperatures would likely have been lower.

The calculated and experimental Mod-1 behavior of the system hydraulics was similar up to the time of gas injection from the accumulators. The flow from the ruptured steam generator tubes blocked normal flow in loop 2 of the calculational model and in the intact loop of the Mod-1 system. Part of the flow entered the upper plenum and traveled preferentially in a specific channel downward into the lower plenum. In

the calculational model the flow path was in vessel cell 7, a cell in the inner core ring just opposite the loop 2 hot leg. In the Mod-1 system, the flow path was the vessel wall on the side adjacent to the intact loop hot leg. This particular path was attributed to the fact that the heater rods extended through the upper plenum thus limiting the penetration of fluid across the core.

For the small rupture experiment the downcomer of the Mod-1 system became blocked at the start of accumulator gas injection stopping the negative core inlet flow and intact loop hot leg flow and forcing liquid into the lower plenum. The calculated results for the small rupture did not show blockage of the downcomer but did result in significant liquid entering the lower plenum. After gas injection, the lower plenum continued filling. In the Mod-1 system the refill rate was less than supplied by the LPIS system, in the PWR model the refill rate was larger and reflooding at the core bottom occurred earlier than for the experiment.

For the large rupture, the rupture flow was sufficient to sweep the liquid out of the downcomer to the broken cold leg for both the calculation and the experiment. The nitrogen gas injection in the Mod-1 system resulted in a reduction in the negative flow rate into the upper plenum. The gas forced subcooled liquid out of the upper portion of the downcomer eliminating the potential for condensation and thus reducing the driving head for negative flow. The gas discharged from the accumulator during the calculation was water vapor which apparently condensed instead of driving any subcooled liquid from the downcomer. Refill of the lower plenum was prevented until the termination of rupture flow in the Mod-1 system and a reduction in the rupture flow rate to about 250 kg/s in the calculation.

### 3.3.2 Core Thermal Response

For the small rupture quenching was initiated in the Semiscale Mod-1 experiment prior to reflooding. It occurred on a few rods near the preferential flow path and near the core midplane. Other locations

quenched after reflooding was initiated. The quench front originated at the core bottom and proceeded upward. The calculated results indicated that the preferential flow was not sufficient to cause quenching before bottom flooding. Af' bottom flooding began a falling film quench front was initiated at the core top as well as a bottom quench front.

For the large rupture, the rupture flow in the Mod-1 system,resulted in quenching from the core top prior to bottom flooding. In the calculation quenching was initiated at the core top but except for vessel cell 7 the falling film receded as the rupture flow diminished prior to reflooding.

Because of the differences in quench behavior between the experiment and the PWR calculation, the results concerning the maximum cladding temperature were different. The experiments resulted in a maximum peak cladding temperature being achieved during the small rupture test. The results of the calculation indicated that peak cladding temperatures were roughly the same for each rupture size.

# 4. CONCLUSIONS AND RECOMMENDATIONS

An investigation using the TRAC-P1A computer program to calculate the behavior of a PWR exposed to a simulated cold leg break with a simultaneous steam generator tube rupture was completed.

1. *The code proved capable of making the detailed calculations of the system hydraulic and core thermal response during the postulated transient.*

2. *Comparisons of the calculations with experimental results from the Semiscale Mod-1 system indicate that the code is correctly calculating the major controlling hydraulic phenomena that occur during a steam generator tube rupture.*

3. *The calculated tube rupture flow exhibited significant three dimensional effects upon entering the upper plenum.*

   The portion of liquid entering the upper plenum from the ruptured tubes flowed in a preferential channel from the upper plenum through the core to the lower plenum. Preferential flow was also observed in the Mod-1 system but may have been caused by the hardware design of the system.

4. *Comparisons of the calculations with the Mod-1 results indicated differences in the core thermal behavior.*

   For the small rupture, the calculation and data indicated that quenching began at the core bottom after refill of the lower plenum was completed. For the large rupture, the calculation indicated that complete quenching would occur as the result of bottom flooding. However, the data indicated that the large rupture flow rate was sufficient in magnitude and distribution

across the core top to cause complete quenching by a falling film prior to lower plenum refill. This difference between calculation and data might be due to the small scale of the experiment not permitting three dimensional effects or because the quench model in the code was not sufficiently sensitive. Analysis of the liquid distribution across the core top would be necessary to evaluate the difference further.

5. *Explicit representation of the 4 loops in the TRAC PWR model is probably not necessary for calculating the system-hydraulic behavior of a postulated LOCA including ruptured steam generator tubes.*

The calculated system hydraulic phenomena agreed reasonably well with the phenomena exhibited by the two loop Semiscale Mod-1 system. Minor differences between the calculation and data occurred, but could be attributed to differences between modeling assumptions and hardware design and operation.

6. *The steam generator component model did not perform satisfactorily during steady state.*

Neither a steady state heat balance nor a mass balance could be obtained using the prescribed boundary conditions. The secondary side temperature had to be reduced by lowering the exit pressure and the secondary side mass flow rate had to be increased to prevent mass depletion. The void fraction distribution in the secondary side was skewed with too much liquid in the middle cells. The result of these effects was likely small for the calculations reported.

## REFERENCES


1. TRAC-P1A, An Advanced Best-Estimate Computer Program for PWR LOCA Analysis, LA-7777-MS, May 1979.

2. P. D. Wheatley and M. A. Bolander, TRAC-P1A Calculations For a 200%, 0.25 m Diameter, and 0.1 m Diameter Cold Leg Breaks in a Pressurized Water Reactor, EG&G Idaho, Inc., EGG-CAAP-5190, June 1980.

3. M. A. Bolander, TRAC-P1A Calculations for a 200% Hot Leg Break and a 200% Hot Leg Break Simultaneous with a Rupture of 16 Steam Generator Tubes in a Pressurized Water Reactor, EG&G Idaho, Inc., EGG-CAAP-5191, June 1980.

4. J. M. Cozzuol, O. M. Hanner, G. G. Loomis, Investigation of the Influence of Simulated Steam Generator Tube Ruptures During Loss-of-Coolant Experiments in the Semiscale Mod-1 System, TREE-NUREG-1213, May 1978.

5. G. W. Johnsen et al., A Comparison of "Best Estimate" and Evaluation Model" LOCA Calculations; The BE/EM study, EG&G Idaho, Inc., Report PG-R-76-009, December 1976.

6. Zion Station Final Safety Analysis Report, Commonwealth Edison Company, Docket No. 50-295 (with amendments).

7. J. Sicilian, "TRAC Newsletter, Number 1", Los Alamos Scientific Laboratory, July 1979.

8. J. C. Vigil et al., TRAC-P1A Developmental Assessment, LA-8056-MS, October 1979.

# APPENDIX A

## NODALIZATION OF MODEL COMPONENTS

# APPENDIX A

## NODALIZATION OF MODEL COMPONENTS

The following describes the nodalization of the vessel, pressurizer accumulators, breaks, ECC injection and steam generator rupture.

### 1. VESSEL

The axial and radial noding of the vessel is shown in Figure A-1. The nodalization consisted of 12 axial levels with each level subdivided into 3 radial and 8 azimuthal zones for a total of 288 mesh cells. The noding was revised several times as improved values for volumes, areas and masses were calculated. The noding is somewhat different than used in the BE/EM[A-1] or USPWR1[A-2] models. Table A-1 shows the vessel fluid volumes, heat slab areas, and heat slab masses used in these calculations.

The downcomer region was modeled by the outer ring between levels 3 and 10. The downcomer lumped two actual flow paths on each side of the thermal shield. The barrel-baffle region which provides an additional flow path parallel to the downcomer was not included explicitly in the model. Its volume, surface area and mass were evaluated in the outer core ring. The flow path was not included.

The lower plenum was noded as three levels. The portion below the downcomer was divided into 2 levels to permit backflow from the core to the downcomer without removing residual liquid from the bottom of the vessel. Level 3 of the lower plenum lies at the bottom of the active core and included structures such as the core support plate and core mixing plate.

The core consisted of 5 axial levels and 2 radial rings. The top of vessel level 8 corresponded to the top of the active fuel. This noding provided a means to represent a axial and radial power distribution in the core. The distributions are tabulated in a later section.

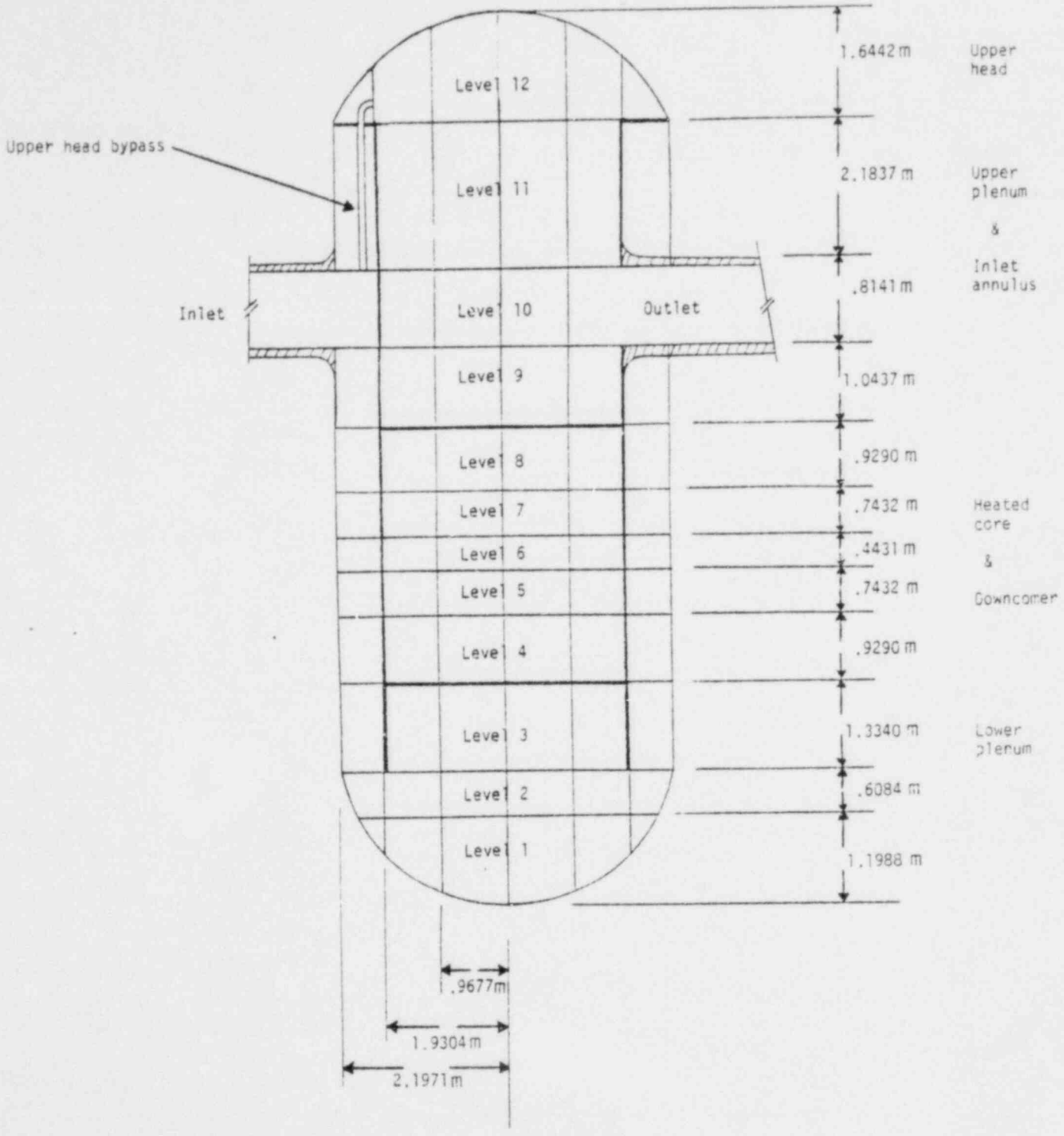


Figure A-1. Axial and radial nodalization of vessel.

TABLE A-1. COMPARISON OF VESSEL VOLUMES, HEAT SLAB AREAS AND HEAT SLAB MASSES

| Lower Plenum Heat Slab Area ($m^2$) | Lower Plenum Heat Slab Mass (kg) | Lower Plenum Liquid Volume ($m^3$) | Downcomer Liquid Volume, Core Section ($m^3$) | Core Liquid Volume ($m^3$) | Downcomer Heat Slab Area, Core Section ($m^2$) |
|---|---|---|---|---|---|
| 180.32 | 29160.0 | 28.57 | 9.68 | 18.32 | 195.79 |

| Core Heat Slab Area ($m^2$) | Core Heat Slab Mass (kg) | Upper Plenum Volume ($m^3$) | Upper Plenum Heat Slab Area ($m^3$) | Inlet Annulus Volume ($m^3$) | Upper Head Volume ($m^3$) | Loop Flow Volume ($m^3$) |
|---|---|---|---|---|---|---|
| 717.73 | 10306.0 | 40.31 | 329.62 | 9.31 | 13.67 | 42.69 |

The fuel rod was divided into 9 cells for the fuel, one cell for the pellet-cladding gap and one cell for the cladding. A radial power distribution was input to the fuel pellets and is described in a following section.

The upper plenum was noded as three levels, level 9 below the inlet and outlet nozzles, level 10 which was sized to span the outlet nozzle flow area, and level 11 above the nozzles and below the upper head. Level 12 represented the upper head region of the vessel.

## 2. PRESSURIZER AND ACCUMULATORS

Figure A-2 shows the cell nodalization used for the pressurizer. The accumulators were nodalized in a similar manner. This type of model was recommended for the pressurizer at the TRAC Workshop[A-3] held at LASL in February, 1980.

Basically, the bottom of the pressurizer and accumulators was modeled by a very short node. The connecting cell of the joining tee was also noded the same length as the adjoining pressurizer or accumulator cell but with a flow area equal to that of the pressurizer or accumulator. The appropriate initial liquid volume was obtained by including the connecting tee cell volume as part of the desired pressurizer or accumulator component volume. The fully implicit hydrodynamics option differencing technique was used on the secondary side of the tee to avoid Courant limiting of the time step size and to provide a better representation of the pressure drop calculated at the junction of the components. Too high a pressure drop and a smaller mass flow rate would be calculated at the junction using the semi-implicit hydrodynamics option if the tee cell was small in diameter compared to the pressurizer cell. Table A-2 shows the pressurizer and accumulator volumes.

Based on the calculated results for the accumulators compared to the Semiscale data, the modeling of the accumulators was not satisfactory. Better comparisons between calculation and data were obtained by not using this technique.[A-4]

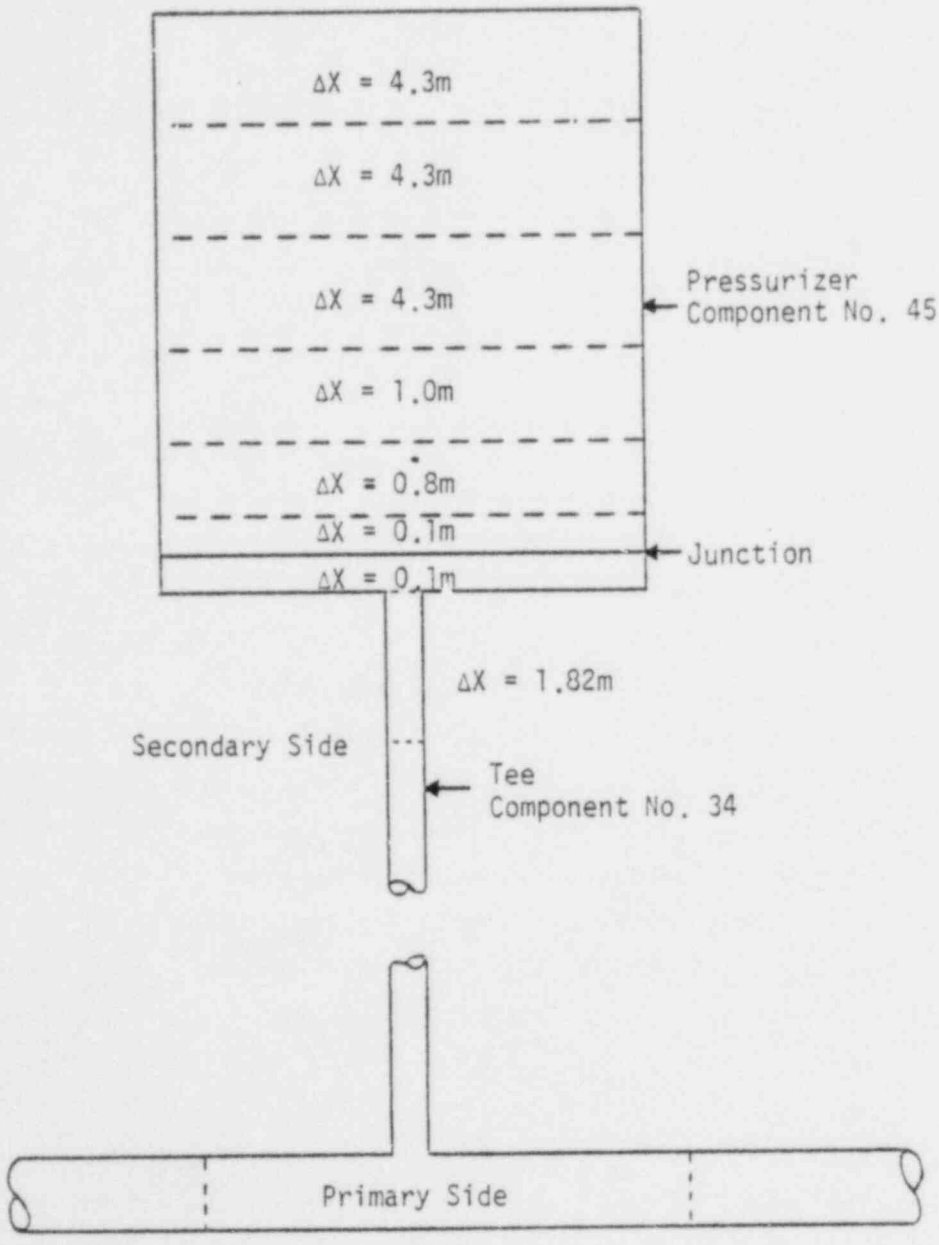


Figure A-2. Nodalization of pressurizer and connecting Tee showing all cell lengths.

## 3. BREAKS

The break piping was nodalized following the guidelines presented in the TRAC-P1A Developmental Assessment Report.[A-5] The nodalization is shown in Tables A-3 and A-4 for the hot leg side break TEE 49 and for the cold leg break side PIPE 6, respectively. The 14 cells upstream of the break have the same spacing. The cold leg break was located just outside the biological shield as was done for the BE/EM study. The length available for the hot leg break piping was determined by the location of the ECC fill component.

A short test run was made with a courser spacing, but little change was noted. Thus it was felt that the selected nodalization was adequate.

## 4. ECC INJECTION

The fill components for each loop lumped together the charging, low pressure, and high pressure systems. The mass flow rates were specified to be equal for each loop and were a function of the local pressure. The mass flow rate as a function of pressure was taken from the BE/EM study for the intact loop and converted to velocity for input to the TRAC computer program.

## 5. STEAM GENERATOR RUPTURE

The TRAC code steam generator component model does not permit direct simulation of a tube rupture permitting flow communication between the primary and secondary sides. Thus, to simulate ruptured tubes at the tube sheet on the inlet side of the steam generator a VALVE component 61 was connected to TEE 12 as shown in Figure A-3. The component model of the steam generator and valve was used to investigate potential problems with the configuration and size the valve opening to obtain the appropriate mass flow rate. The component consisted of a converging-diverging nozzle with a valve to provide a means of adjusting the flow area.

TABLE A-2. PRESSURIZER AND ACCUMULATOR VOLUMES

| Pressurizer Volume ($m^3$) | Accumulator Volume ($m^3$) |
|---|---|
| 30.32 | 26.88 |

TABLE A-3. BREAK TEE 49 NODALIZATION

| Cell No. | | Length (m) |
|---|---|---|
| 1 | Junction cell | 0.25 |
| 2 | | 0.25 |
| 3 | | 0.15 |
| 4 | | 0.15 |
| 5 | | 0.10 |
| 6 | | 0.10 |
| 7 | | 0.06 |
| 8 | | 0.06 |
| 9 | | 0.04 |
| 10 | | 0.04 |
| 11 | | 0.03 |
| 12 | | 0.03 |
| 13 | | 0.025 |
| 14 | Break junction | 0.025 |

Total length equals 1.31 m.

TABLE A-4. BREAK PIPE 6 NODALIZATION

| Cell No. | Length (m) |
|---|---|
| 1 Break junction | 0.025 |
| 2 | 0.025 |
| 3 | 0.03 |
| 4 | 0.03 |
| 5 | 0.04 |
| 6 | 0.04 |
| 7 | 0.06 |
| 8 | 0.06 |
| 9 | 0.10 |
| 10 | 0.10 |
| 11 | 0.15 |
| 12 | 0.15 |
| 13 | 0.25 |
| 14 | 0.25 |
| 15 | 0.34 |
| 16 | 0.45 |
| 17 | 0.667 |
| 18 | 0.667 |
| 19 | 0.667 |
| 20 | 0.667 |
| 21 | 0.667 |
| 22 | 0.667 |
| 23 Vessel junction | 0.667 |

Total length equals 6.569 m.

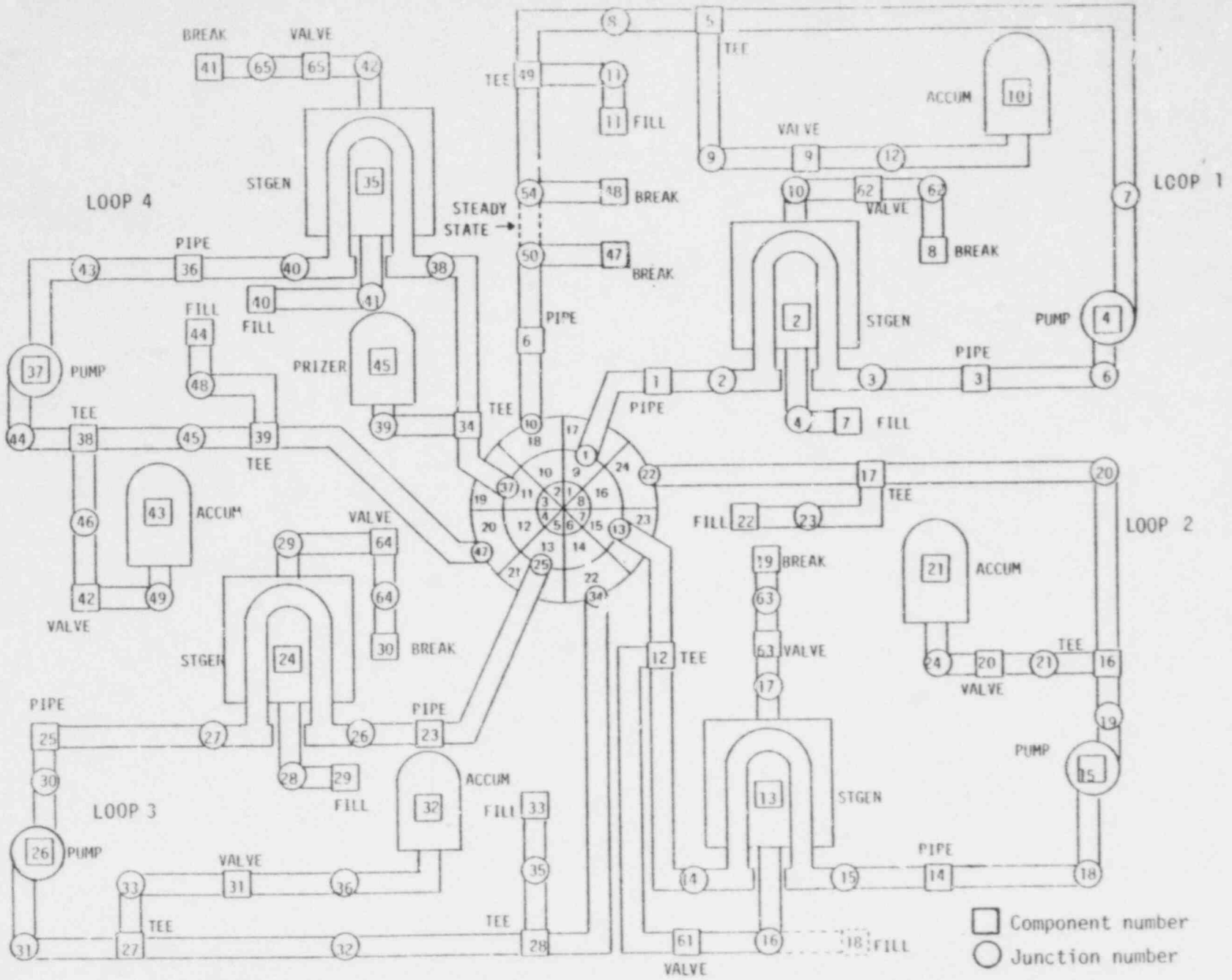


Figure A-3. Nodalization of loops and vessel level 10 for transient calculations.

The appropriate mass flow rate was obtained from Semiscale test results[A-6] which showed a maximum peak cladding temperature for a particular mass flow rate from a simulated rupture in the steam generator. The mass flow rate for the PWR was determined by applying core area scaling to the Semiscale results. Different scaling criteria would lead to different mass flow rates. The Semiscale tests were run from conditions simulating the steam generator and primary system after blowdown. Therefore, the valve area was sized with the primary side of the steam generator and piping kept at 0.25 MPa. The secondary side was initialized at conditions corresponding to steady state operation.

The desired mass flow rate was determined in the following manner for the small rupture. The mass flow rate from 16 ruptured tubes, as determined in the reference, was scaled by the ratio of the Semiscale and PWR core flow areas, ie,

$$\frac{\text{leakage mass flow rate (PWR)}}{\text{core flow area (PWR)}} = \frac{\text{leakage mass flow rate (SS)}}{\text{core flow area (SS)}}$$

Substituting in this ratio and solving for the PWR leakage mass flow rate yielded,

$$9.07^{-3}\ \frac{\text{Kg}}{\text{s}}\ \begin{matrix}\text{scaled}\\ \text{per tube x 16 tubes}\\ \text{for SS}\end{matrix} \quad x\ \frac{4.933\ m^2\ \text{(Zion I core flow area)}}{4.768 \times 10^{-3} m^2\ \text{(Semiscale core flow area)}}$$

$$= 150.1\ \frac{\text{Kg}}{\text{s}}$$

Figure A-4 shows the geometry of the symmetric nozzle for the small rupture.

The mass flow rate for the large rupture calculation was the largest mass flow rate tested in Semiscale. This corresponded to about 600 kg/s using the same scaling technique.

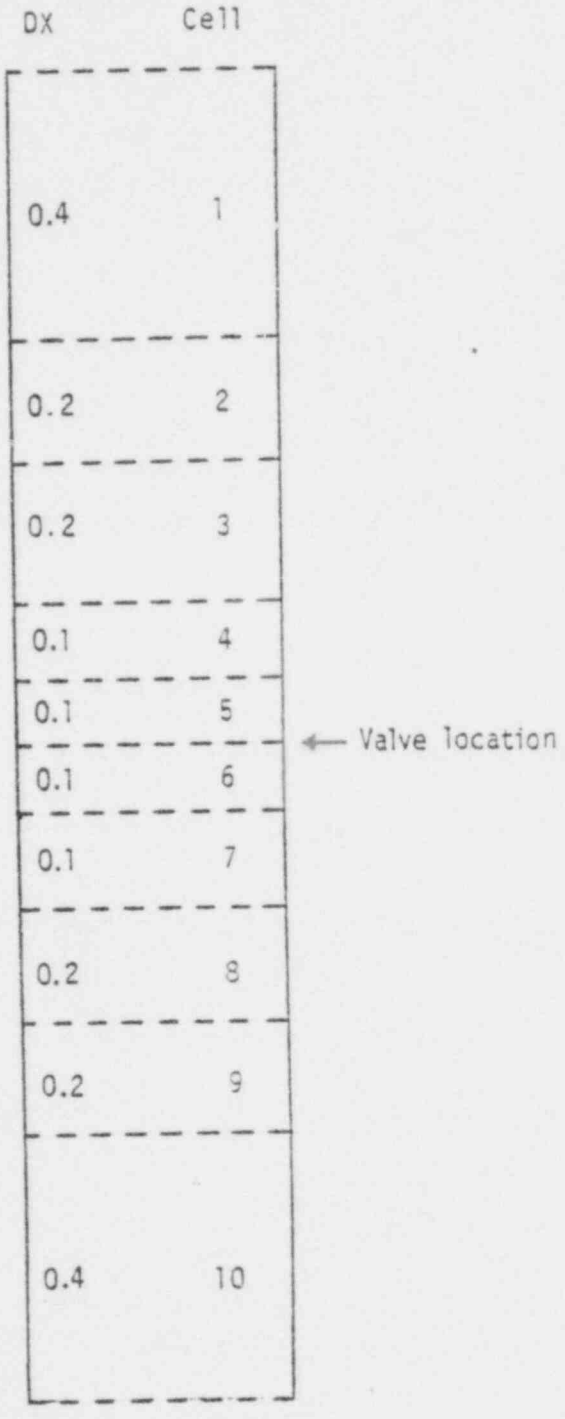


Figure A-4. Nodalization of valve simulating small number of steam generator ruptured tubes.

To obtain the correct heat transfer from the primary side to the secondary side of the steam generator it was necessary to lower the back-pressure at the secondary side break from 5.24 to 4.6 MPa. Also to obtain a steady state mass balance across the secondary side it was necessary to increase the inlet mass flow to about 800 kg/s from the specified 440.7 kg/s.

## REFERENCES


A-1. G. W. Johnsen et al., A Comparison of "Best Estimate" and "Evaluation Model" LOCA Calculations: The BE/EM Study, EG&G Idaho, Inc., Report PG-R-76-009, December 1976.

A-2. TRAC-P1A, An Advanced Best Estimate Computer Program for PWR LOCA Analysis, LA-7777-MS, May 1979.

A-3. J. K. Meier, "Problem Modeling", TRAC Workshop, Los Alamos, New Mexico, February 6, 1980.

A-4 P. N. Demmie, An Analysis of Semiscale Mod-1 LOCE S-04-6 Using the TRAC-P1A Computer Program, EG&G Idaho, Inc., EGG-CAAP-5181, June 1980.

A-5. J. C. Vigil et al., TRAC-P1A Developmental Assessment, LA-8056-MS October 1979.

A-6. J. M. Cozzuol, O. M. Hanner, G. G. Loomis, Investigation of the Influence of Simulated Steam Generator Tube Ruptures During Loss-of-Coolant Experiments in the Semiscale Mod-1 System, TREE-NUREG-1213, May 1978.

# APPENDIX B

# COMPONENT INITIAL AND BOUNDARY CONDITIONS

APPENDIX B

# COMPONENT INITIAL AND BOUNDARY CONDITIONS

This section describes the initial and boundary conditions of the model components.

## 1. CORE POWER DISTRIBUTION

The relative axial power distribution for the 5 core levels is tabulated in Table B-1. The distribution is very similar to the BE/EM study.[B-1] Slight differences occurred because the BE/EM study included vessel structure and volume above and below the active core in the top and bottom core volumes and the core was divided into 6 core levels.

The relative core radial distribution is shown in Table B-2. The distribution was obtained from a report on Zion I fuel performance[B-2] by averaging the peaking factors given for each fuel assembly within the inner and outer rings of the model corresponding to the core. The axial and radial distributions resulted in an average rod peak steady state power generator of 31.73 Kw/m (9.67 Kw/ft). The decay heat generation was based on the ANS specification and was taken from the BE/EM study.

The relative fuel rod radial power distribution is shown in Table B-3. the distribution was obtained from Reference B-2.

## 2. PUMPS

The primary loop circulating pumps were left on throughout the transient calculation.

TABLE B-1. RELATIVE CORE AXIAL POWER DISTRIBUTION

| Core Level | Factor |
|---|---|
| 1 bottom | 0.8142 |
| 2 | 1.189 |
| 3 | 1.20 |
| 4 | 1.1706 |
| 5 top | 0.7018 |

TABLE B-2. RELATIVE CORE RADIAL POWER DISTRIBUTION

| Ring | Factor |
|---|---|
| 1 inner | 1.0898 |
| 2 outer | 0.83373 |

TABLE B-3. RELATIVE FUEL ROD RADIAL POWER DISTRIBUTION

| Node | Factor |
|---|---|
| 1 centerline | 0.967 |
| 2 | 0.969 |
| 3 | 0.972 |
| 4 | 0.977 |
| 5 | 0.984 |
| 6 | 0.992 |
| 7 | 1.003 |
| 8 | 1.016 |
| 9 | 1.037 |

## 3. SAFETY INJECTION FLOW

The safety injection and charging systems were combined into one fill for each loop. The mass flow injected as a function of local pressure is shown in Figure B-1.

## 4. STEAM GENERATORS

Steam flow from the secondary side of the steam generators was shut off at 1.5 s by linearly closing the valve upstream of the break. This was necessary to prevent steam backflow into the steam generator as the secondary side pressure dropped below the exit pressure. The feedwater was terminated and auxiliary feed was begun as shown in Figure B-2. The initial conditions for the secondary side of the steam generators listed in Table B-4. The initial void fraction distribution and mass inventory could not be adjusted to obtain desired distribution or inventory.

## 5. SCRAM

Scram occurred at 0.53 s.

## 6. CONTAINMENT PRESSURE

The containment pressure is shown as a function of time in Figure B-3.

## 7. ACCUMULATORS AND PRESSURIZER

The initial conditions for the accumulators and pressurizer are listed in Table B-5.

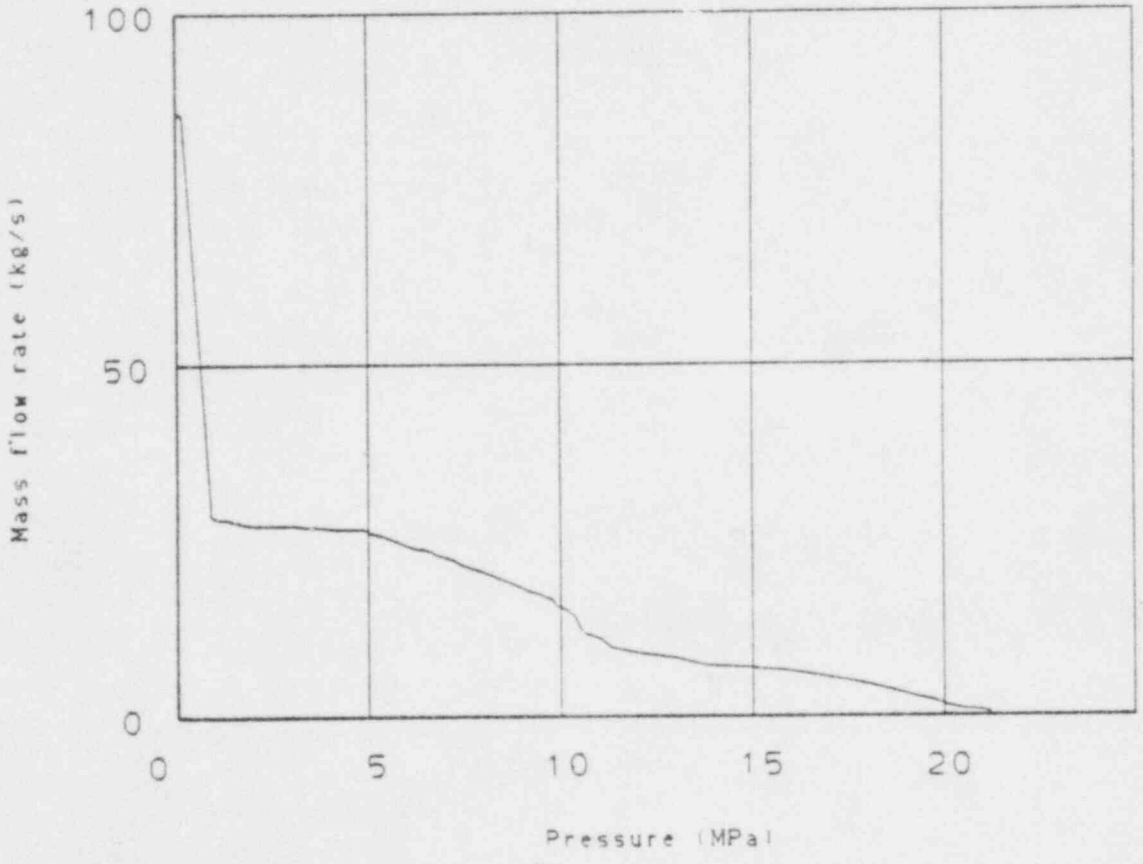


Figure B-1. ECC injection mass flow rate.

TABLE B-4. INITIAL CONDITIONS FOR ZION I STEAM GENERATOR SECONDARY SIDE COMPARED TO THE BE/EM STUDY

| | ZION I | BE/EM |
|---|---|---|
| Back Pressure (MPa) | 4.6 | 5.25 |
| Inlet Temperature (K) | 493.0 | 493.0 |
| Mass (kg) | 51,500.0 | 40,000.0 |

TABLE B-5. INITIAL CONDITIONS FOR ACCUMULATORS AND PRESSURIZER

| | Accumulators | Pressurizer |
|---|---|---|
| Pressure (MPa) | 4.43 | 15.43 |
| Temperature (K) | 325.0 | 598.0 |
| Trip Pressure (MPa) | 4.08 | |

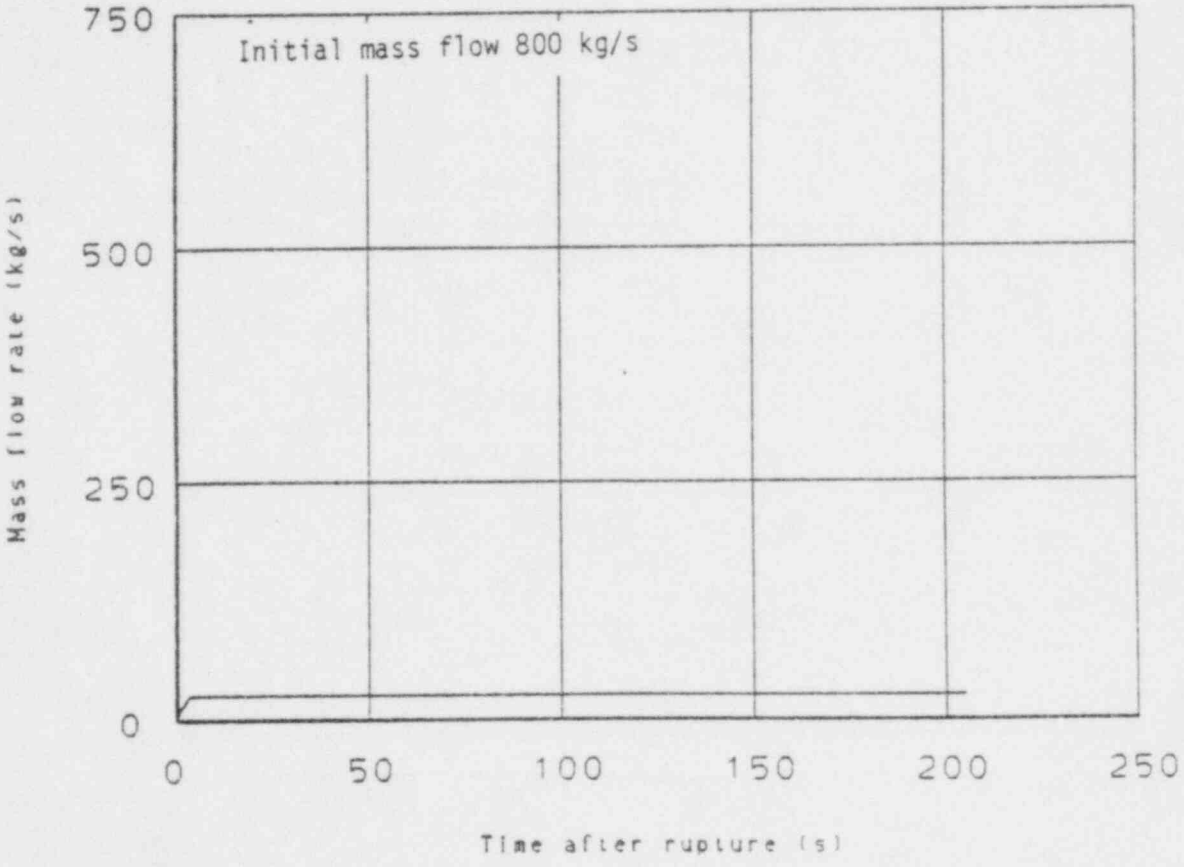


Figure B-2. Steam generator feedwater and auxiliary feedwater mass flow.

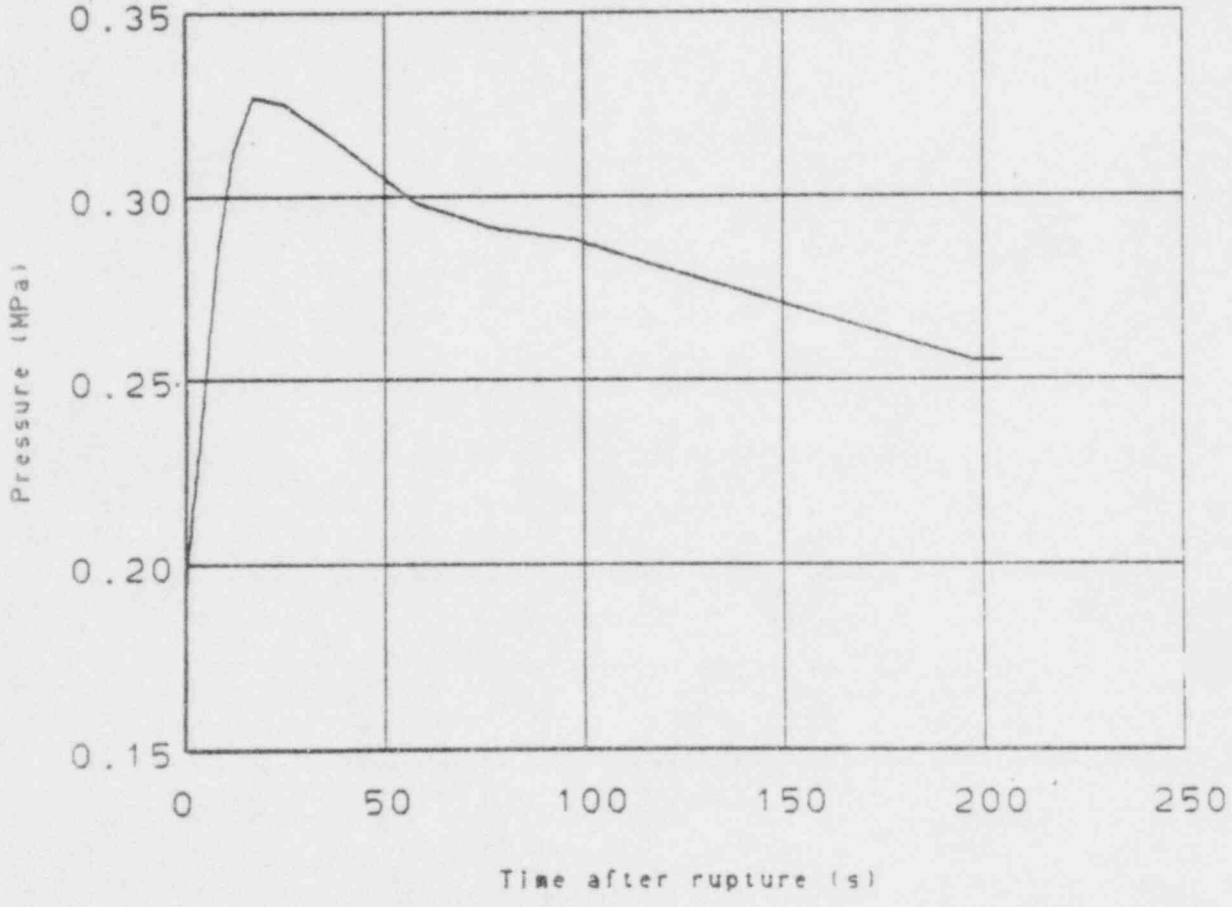


Figure B-3. Containment pressure.

# REFERENCES


B-1. G. W. Johnsen et al., A Comparison of "Best Estimate" and Evaluation Model" LOCA Calculations; The BE/EM study, EG&G Idaho, Inc., Report PG-R-76-009, December 1976.

B-2. H. H. Crain et al., Interim Report, Zion Unit 1, Cycle 1 Fuel Performance, Westinghouse Electric Corporation, WCAP-8837 December 1976.

# APPENDIX C

## CODE INPUT LISTING

# APPENDIX C

## CODE INPUT LISTING

The following contains the steady state conditions for all components and the changes for the two transient calculations.